Nanoelectronics-Biology Frontier: From Nanoscopic Probes for Action Potential Recording in Live Cells to Three-Dimensional Cyborg Tissues

Review

Nanoelectronics-biology frontier: From nanoscopic probes for action potential recording in live cells to three-dimensional cyborg tissues

Xiaojie Duan[1,2*], Tian-Ming Fu[2], Jia Liu[2], Charles M. Lieber[2,3*]

[1]*Department of Biomedical Engineering, College of Engineering, Peking University, Beijing 100871, China*

[2]*Department of Chemistry and Chemical Biology, and* [3]*School of Engineering and Applied Sciences, Harvard University, Cambridge, Massachusetts, 02138, USA.*

*Corresponding authors. Tel.: +86 10 6276 7113; E-mail address: xjduan@pku.edu.cn (X. Duan); and Tel.: +01 617 496 3169; E-mail address: cml@cmliris.harvard.edu (C. M. Lieber).

Keywords: bioelectronics, nanowire, nanodevice, field-effect transistor, brain activity mapping, macroporous 3D electronics, flexible electronics, synthetic tissue, cellular and subcellular resolution, graphene

Summary Semiconductor nanowires configured as the active channels of field-effect transistors (FETs) have been used as detectors for high-resolution electrical recording from single live cells, cell networks, tissues and organs. Extracellular measurements with substrate supported silicon nanowire (SiNW) FETs, which have projected active areas

orders of magnitude smaller than conventional microfabricated multielectrode arrays (MEAs) and planar FETs, recorded action potential and field potential signals with high signal-to-noise ratio and temporal resolution from cultured neurons, cultured cardiomyocytes, acute brain slices and whole animal hearts. Measurements made with modulation-doped nanoscale active channel SiNW FETs demonstrate that signals recorded from cardiomyocytes are highly localized and have improved time resolution compared to larger planar detectors. In addition, several novel three-dimensional (3D) transistor probes, which were realized using advanced nanowire synthesis methods, have been implemented for intracellular recording. These novel probes include (i) flexible 3D kinked nanowire FETs, (ii) branched intracellular nanotube SiNW FETs, and (iii) active silicon nanotube FETs. Following phospholipid modification of the probes to mimic the cell membrane, the kinked nanowire, branched intracellular nanotube and active silicon nanotube FET probes recorded full-amplitude intracellular action potentials from spontaneously firing cardiomyocytes. Moreover, these probes demonstrated the capability of reversible, stable, and long-term intracellular recording, thus indicating the minimal invasiveness of the new nanoscale structures and suggesting biomimetic internalization via the phospholipid modification. Simultaneous, multi-site intracellular recording from both single cells and cell networks were also readily achieved by interfacing independently addressable nanoprobe devices with cells. Finally, electronic and biological systems have been seamlessly merged in 3D for the first time using macroporous nanoelectronic scaffolds that are analogous to synthetic tissue scaffold and the extracellular matrix in tissue. Free-standing 3D nanoelectronic scaffolds were cultured with neurons, cardiomyocytes and smooth muscle cells to yield electronically-

innervated synthetic or 'cyborg' tissues. Measurements demonstrate that innervated tissues exhibit similar cell viability as with conventional tissue scaffolds, and importantly, demonstrate that the real-time response to drugs and pH changes can be mapped in 3D through the tissues. These results open up a new field of research, wherein nanoelectronics are merged with biological systems in 3D thereby providing broad opportunities, ranging from a nanoelectronic/tissue platform for real-time pharmacological screening in 3D to implantable 'cyborg' tissues enabling closed-loop monitoring and treatment of diseases. Furthermore, the capability of high density scale-up of the above extra- and intracellular nanoscopic probes for action potential recording provide important tools for large-scale high spatio-temporal resolution electrical neural activity mapping in both 2D and 3D, which promises to have a profound impact on many research areas, including the mapping of activity within the brain.

Introduction

Large-scale and high spatial resolution cellular and subcellular-level interfaces between electrical sensors and biological systems are crucial for both fundamental biophysical studies and medical monitoring and intervention [1-5]. For example, the exploration of the brain function depends largely on the development of new tools that can simultaneously measure and manipulate the electrical activity of thousands or even millions of neurons with high spatial and temporal resolution. Over the past several decades, a variety of electrical probes including glass micropipette intracellular and patch-clamp electrodes [1,4,5], multielectrode arrays (MEAs) [2,4,6-8], and planar

field-effect transistors (FETs) [9-12] were developed and widely used to record action potentials and transmembrane potential changes from electroactive cells and tissues, as well as to probe chemical events at the surface of tissues or individual cells. These probes, which are normally micrometer in size, can readily interface with cellular level resolution and provide valuable information on cell network function. However, the size of these probes poses a challenge to record from small subcellular structures or to carryout simultaneous, large-scale multi-site recording with subcellular-level resolution [10,13-16].

The intense interest placed in recent years on chemically-synthesized semiconductor nanowires has led to the development of a broad range of structures with rationally controlled geometry, composition, and electronic properties [17-21]. As predictable and synthetically well-controlled structures, semiconductor nanowires have been used as powerful building blacks for the bottom-up assembly of functional devices such as FETs, photodetectors, and photodiodes [18,19,22,23]. Nanoscale functional devices such as nanoFETs can be used as voltage and chemical sensors thereby enabling new classes of molecular scale electronic interfaces with biological systems [24-29]. Compared to conventional glass micropipettes, sharp metal electrodes, or microfabricated MEAs and planar FETs, there are two major advantages of these new nanoFET based sensors. First, the small size of these probes (Fig. 1a) allows for simultaneous multi-site recording with increased number and density of recording sites, which enables larger scale and higher spatial resolution, and also intracellular measurements that are much less invasive to cells [27-29,32,33]. In addition, the small size also enables more localized, higher spatial precision measurements, which is necessary for subcellular level

interfacing, for example, in measurements from neurites [27,30,31]. Second, the intrinsic strength of bottom-up assembly (Fig. 1b) allows semiconducting nanowire functional elements to be assembled on nearly any type of surface, including those that are typically not compatible with standard CMOS processing, such as flexible plastic substrates [23,34-38]. Moreover, sequential patterning and assembly steps further enable fabrication of distinct nanowire nanodevices on a substrate (Fig. 1b) to incorporate multi-function in measurement chips [37]. Last, bottom-up assembly of nanowires enables the fabrication of flexible, free-standing devices [28,39]. Three-dimensional (3D), free-standing, macroporous device array can be utilized as the scaffolding for synthetic tissue constructs and used to monitor cellular activity throughout 3D cellular networks [39], capabilities that are not accessible with conventional electrode probes or even recently developed flexible electronics [36,40,41].

In this review, we will describe the development of new biological sensing devices using semiconducting nanowires as the probe structure and detector or nanowire based structures as the functional detector element, as well as their application in extracellular and intracellular measurements. Specific emphasis will be placed on transmembrane and action potential recording from living biological systems ranging from cultured cells, acute tissue slices, and whole organs through synthetic nanoelectronic/tissue constructs. The uniqueness enabled by the use of nanometer scale functional semiconducting nanowires will be highlighted, and exciting future applications of these new probes in biophysical and electrophysiological studies will be discussed.

Extracellular electrical recording

The potential change outside the cells associated with the transmembrane change of excited cells can be recorded by metal or glass micropipette electrodes to monitor the electric activity of the cells [2,6,7,11]. Compared to intracellular recording, which normally places the tip of the probe structure inside the cells, extracellular recording is less invasive and provides ready access to simultaneous multi-site recording such as using MEAs [2,6,7]. The size of the metal electrodes used in extracellular recording is normally 5-100 microns [2,6,7,14]. This relatively large size ensures a reasonable impedance value at the electrode/electrolyte interface and gives sufficient signal-to-noise ratio (SNR) for action potential detection. Extracellular recording with MEAs has been used in many studies including development of electric activity and dynamics study in cultured neuron networks [42], neuronal activity in brain slices [43] and photo response of the networks in the retina [44]. However, the large size and corresponding low spatial resolution of MEAs make it difficult to record from critical subcellular structures, such as axons and dendrites [16]. The large size also makes cell-to-electrode registration challenging because measured signals for a given electrode typically are due to contributions from several nearby cells. As a result, identification of specific cellular signals from MEAs recording generally requires complicated post-processing, such as the spike sorting [6,7].

In this regard, nanoscale devices can provide distinct advantages by realizing subcellular-scale interfaces between recording probes and biological systems, and enabling precise cell-to-electrode registration. FETs using chemically synthesized

semiconductor nanowires as functional channels (Fig. 2a) are good candidates for this purpose. As shown in Fig. 2b, when putting a SiNW FET in electrophysiology medium [45], it exhibits a conductance change in response to variations of the solution potential. The FETs are normally referred as active potential detectors, in distinction to the passive metal electrodes. The solution acts as analog of metallic gate electrode in the conventional FET configuration, and thus is termed a water-gate [24, 45]. Because potential sensing with FETs is not dependent on solution/device interface impedance [45,46], there is no fundamental limitation (in contrast to MEAs) on reducing the size of FET-based detectors to the nanometer scale. In our nanowire FET sensors, the diameter of nanwires is normally in the range of 10-100 nm, and the channel length of the FET is in the range of 50-2000 nm. Compared to their planar counterparts, NWFETs are expected to be more sensitive detectors due to the one-dimensional (1D) nanoscale morphology; that is, the potential change on the surface of a nanowire leads to depletion or accumulation of carriers in the "bulk" of the 1D nanometer-diameter structure, versus only a shallow region near the surface in the case of a planar device. The exquisite sensitivity, combining the nanoscale size, makes NWFETs appealing as extracellular recording probes with cellular or subcellular-level resolution.

Extracellular recording from cultured cells using SiNW FETs

The first demonstration of using nanoscale FETs as extracellular recording probes for electroactive biological systems was carried out on cultured rat cortical and hippocampal neurons [27]. By using surface patterning of poly-lysine on NWFET device chips, the neuron cells, including both the cell body and neurites, were selectively grown

to ensure a high yield of neuron/nanowire junctions and hence an efficient interfacing. Figure 3a [27] shows an optical image of a cortical neuron interfaced with a NWFET with the axon aligned across the nanowire channel. The signal recorded by this p-type NWFET was in good temporal correlation with the intracellular action potentials recorded by a glass micropipette (Fig. 3b) [27]. This direct correlation indicates that the depolarization of cell membrane during action potential firing results in negative charging of the extracellular space around the nanowire. This is consistent with the fact that the membrane expresses a relatively high density of Na^+ ion-channel [47-49]. Key advantages demonstrated by this work include (1) the straightforward recording of action potential signals from individual neurites, which is difficult at best from MEAs due to their large electrode size, and (2) the small active junction area for nanowire/axon interfaces, 0.01–0.02 μm^2, which is at least two orders of magnitude smaller than microfabricated electrodes and planar FETs [6,12]. Both advantages highlight the higher spatial precision and resolution of NWFETs.

The high spatial resolution enabled by NWFETs makes possible efficient multiplexed recordings from single neurons. NWFETs can be easily and controllably made in arrays, with density higher than that reported with MEAs and planar FETs [50] . One example of this high density multiplexed recording is shown in Fig. 3c and d [27] . In this work, patterned poly-lysine led to neurite growth from a central neuron soma across three of the four peripheral SiNW devices arranged at the corners of a rectangle, as shown in Fig. 3c. Signals were recorded from the three SiNW FETs interfaced with the axon (NW1) and dendrites (NW2 and 3), while the fourth FET (NW4), which did not have a neurite crossing the NW, did not show any signal. This result indicates that there

was no crosstalk in the device array. Importantly, multiplexed recording carried out in this way can be used to study spike propagation, like the back propagation of the action potential in dendrites as demonstrated in this work [27].

In addition to direct culture of electroactive cells on NWFET device arrays, we developed a new and more general scheme for investigating the NWFET/cell interface [51]. This method, which is illustrated schematically in Fig. 4a, allows for separate design and optimization of the NWFET array and cell culture such that the two key components are brought together under precise manipulation only during the final measurement phase. For example, embryonic chicken cardiomyocytes were separately cultured on 100-500 μm thick, optically transparent and flexible polydimethylsiloxane (PDMS) pieces to form cell monolayers [51]. Then a PDMS/cardiomyocyte substrate was transferred over the NWFET chip. Using optical microscope and x-y-z manipulator, spontaneously beating cells of interest were positioned over NWFETs (Fig. 4a and b) [51]. This approach enables us to identify, register to and record from specific cellular and subcellular regions with respect to NWFET devices and carry out multiplexed recording from well-defined multicellular configurations with overall subcellular resolution.

With this method, we recorded extracellular signals from spontaneously firing chicken cardiomyocytes [51]. The signal is regularly spaced biphasic spikes with a frequency of 0.5-1.5 Hz, time scale of 1-3 ms (Fig. 4c and d) [51]. All of the spikes correlate with the beating of the cells in time, indicating the signal corresponds to action potential firing of the cells. The peak width is consistent with time scales for ion fluxes

associated with ion-channels opening/closing [52]. The amplitude is normally in the range of 1 to 4 mV, with a SNR routinely > 5. The tunable interface between the PDMS/ cells and devices leads to a tunable signal amplitude and SNR. In our measurements, by bringing the cells closer to devices with a force applied to the PDMS cell support, the signal amplitude can reach a value of 10.5 mV (Fig. 4e) and a maximum SNR of 25 before making irreversible changes and cessation of the spontaneous beating [51]. It should be noted that within this range, the spike amplitude changes are reversible and the NWFET/cell interface is stable for different displacements toward the devices. High resolution comparison of the recorded signals (Fig. 4d) demonstrates that there is no observable change in either peak shape or peak width over a >2x change in amplitude. Recent studies of Aplysia neurons cultured on planar FET devices have also reported an increase in the peak amplitude when the cell body was displaced [11], which is consistent with our results. The enhanced signal amplitudes can be attributed to a decrease in the gap between the cell membrane and NWFET devices, although further studies will be needed to quantify such junction changes.

This new interfacing strategy can also be used for multiplexing measurements, as different devices can all form tight junctions with the cells, and hence simultaneously give signals with high SNR. The time shift between devices derived from the cross-correlation analysis of data traces recorded in this manner provides information about the action potential propagation direction and speed [51]. The flexibility of interfacing with specific cellular areas for high density multiplexed recording using NWFETs represents a powerful platform to study the effects of cell monolayer inhomogeneity on action potential propagation [53,54], enabling both intra- and intercellular propagation to be

characterized in details for well-defined cellular structures.

Extracellular recording with graphene and short-channel nanowire FETs

As discussed above, the small size of NWFETs allows for more localized and higher spatial precision recording than achievable with planar FETs and MEAs. We compared the recording from NWFETs with graphene FETs to investigate how the size of the extracellular recording probe affects the signal. Graphene consists of a single atomic layer of sp^2-bonded carbon atoms and is an interesting nanomaterial that bridges between 1D nanowires and conventional planar electronics [55,56]. Different from doped semiconducting nanowires, graphene exhibits ambipolar behavior; that is, by varying the gate voltage it is possible to transition from p- to n- type behavior as the Dirac point is crossed [55,56]. This unique characteristic of graphene allows both the amplitude and sign of the recorded signal to be tuned by changing the water gate offset.

We fabricated nanowire and graphene (Gra-) FETs on the same chip (see the schematics in Fig. 5a) and interfaced these distinct detectors with spontaneously firing cardiomyocytes as described above to investigate how the size/active detection area of the extracellular probe affects the signal [37]. Figure 5b shows an image of a relatively large Gra-FET with active channel of 20.8 μm × 9.8 μm, while individual extracellular peaks recorded by this device are shown in Fig. 5d [37]. The recorded data are quite reproducible with an average peak-to-peak width of 1310±40 μs. Interestingly, the average peak-to-peak width recorded from a smaller Gra-FET with active channel of 2.4 μm × 3.4 μm (Fig. 5c) is 730±40 μs (upper traces, Fig. 5e), which is almost a factor of

two smaller than that recorded from the larger Gra-FET. Simultaneously recorded signals from a 0.07 μm^2 active area SiNW FET which is 16 μm away from the smaller Gra-FET (Fig. 5c) yields a peak-to-peak width of 760±40 μs (lower trace, Fig. 5e), which is similar to the value for the smaller Gra-FET.

The above results indicate that the signals recorded with the larger Gra-FET do not represent a localized detection but rather an average of the extracellular potential from different parts of the beating cell or even from different cells. As a result, the peak-to-peak width was broadened. The smaller Gra-FET yielded similar peak-to-peak width as the SiNW FET of ~100X smaller active detection area. We attribute the similar peak widths as arising from the micrometer scale channel length of the SiNW FET detector. Although the detection can be localized in nanometer scale in the radial direction, there will still be average from the micrometer long axial detection, which leads to the broadened peaks detected by the SiNW FET compared to the intrinsic values expected for sodium ion channels.

The NWFET can be a "point-like" detector with more localized recording if we further shrink its active channel down to the size comparable to the nanowire diameter. The short channel NWFET can be made by putting the source and drain electrode close using electron beam lithography [57]. However, these metal electrodes will physically limit cell access and also electrostatically screen the active nanowire channel [57], making it less sensitive to the potential change of the solution around it. With chemically synthesized nanowires, the "point-like" ultra-small detector can be realized in a unique way of dopant modulation [17, 58, 59]. By changing the dopant ratio during nanowire

growth, we can synthesize directly short length lightly doped active channels connected to heavily doped nanowire segments that function as nanoscale source/drain electrode arms [20]. Metal interconnects are then placed on these two arms, thus ensuring an intimate contact between the cells and detectors.

To achieve short-channel nanowire devices with a sharp lightly-heavily doped transition between active elements and arms, we used a combination of nanocluster-catalyzed vapor-liquid-solid (VLS) growth [17] and vapor-solid-solid (VSS) [60, 61] as illustrated in Fig. 6a. The slow growth rates during VSS growth, which are at least 10-100 times lower than for VLS growth [62-65], enable control of the lightly-doped nanowire channel segment on a 10 nm scale and abrupt lightly-heavily doped nanowire junctions. SEM imaging of selectively etched lightly-doped nanowire segments (Fig. 6b) showed that nanowires with channel lengths of 150, 80, and 50 nm could be synthesized by design [59]. Extracellular recording from spontaneously firing cardiomyocytes using NWFETs configured from these new short-channel SiNWs (Fig. 6c) yielded action potential signals with peak-to-peak widths of 520 ± 40, 450 ± 80, and 540 ± 50 μs for the 150, 80 and 50 nm devices, respectively [59]. These widths are significantly smaller than the peak-to-peak widths of 750−850 μs recorded with the conventional nanowire and graphene devices with micrometer scale active channels discussed above, and thus indicate the advantage of the recording with "pointlike" detectors to avoid extrinsic temporal broadening. Interestingly, the time scale reported for Na^+ channel conduction is about 500 μs [1], which is consistent with the peak widths measured from the short channel SiNW FETs here. This suggests that our short channel NWFET devices may be able to study ion channel on the length and time scale of single

ion channel events in future studies.

This approach was also exploited to realize high density multiplexed extracellular recording with designed short-channel NWFETs. For example, three ca. 100 nm devices (d1, d2 and d3, Fig. 6d), where d1 and d2 were synthesized on the same nanowire with < 2 μm separation, were used to record extracellular signals from a network of beating cardiomyocytes [59]. Analysis of the data from the three devices (Fig. 6e, f) showed timing difference of 4.9 and 89 μs for the two devices separated by 1.9 μm (d1 and d2) and 73 μm (d1 and d3) respectively [59]. These results highlight that both intra and intercellular signal propagation across the cell network can be recorded with the NWFET arrays.

Extracellular recording from tissue slices and organs

Tissues such as that obtained from the brain and heart, represents more complex biological systems where NWFET devices offer unique opportunities for collect electrophysiological information. In the brain, neural circuits are organized through synaptic connections into hierarchical networks operating on spatial and temporal scales that span multiple orders of magnitude [66]. From this perspective, electrical recording with both high spatial and temporal resolution from populations of neurons using NWFET arrays is highly desirable to map the activities of the neural circuits. On the other hand, electrical recording in vitro and in vivo from whole hearts is important in areas ranging from basic studies of cardiac function to patient healthcare [3,4,67,68]. Bottom-up assembly of nanowires allows fabrication of flexible and transparent recording chips that provide a more powerful way to interface with organs, such as the

heart. In this section, we will review recent progress using NWFETs to record from acute rat brain slices and the whole embryonic chicken hearts.

First, NWFET arrays have been used to record neuronal network activity from acute brain slices [69] as shown schematically in Fig.7a. An optical image of an oriented acute brain slice (Fig. 7b) shows the lateral olfactory tract (LOT) (*Dark Band*) and the pyramidal neuron layers. A schematic of the organization and circuit of the slice (Fig. 7c) highlights the LOT and synaptic connections (*Layer I*) with the pyramidal cells in *Layers II* and *III*, which are oriented over the NWFET array (Fig. 7b). Following stimulation on the LOT, two types of signals were recorded from NWFETs [69]. When a NWFET is close to the somata of pyramidal neuron the signal showed a positive excitatory postsynaptic potential (EPSP, marked by +, Fig. 7d) followed by a population spike (p-spike) [69]. However, when the NWFET was close to dendritic projections, a broad negative potential change with less significant p-spike on the tail was detected (lower trace, Fig. 7d). The distinct signals reflect the different change of the extracellular potential at different local regions of pyramidal cells, which correspond to current sources and sinks in the neural network [66].

Significantly, differences in the recorded signal were observed between devices with spacing as small as 5 μm, which exceeds substantially that reported in previous MEAs and planar FETs measurement [43,70-72], thus demonstrating the high spatial resolution of the NWFET detection. The high resolution recording capability of NWFET 2D arrays was exploited to map the neural connectivity in the olfactory cortex. Representative data recorded from eight devices following stimulation at eight different

spots (a-h, Fig. 7b) in the LOT showed distinct responses (Fig. 7e). Specifically, the 2D maps from the NWFET array resolved clearly the heterogeneous activity of the neural circuit [69]. We note that the distance between adjacent devices, 60 μm, in which distinct activity was recorded is already better than the 100 μm scale resolution achieved in MEAs recording of brain slices [43, 71], although in our case the mapping resolution can be substantially improved by using higher density NWFET arrays [50].

For whole heart recording, macroscale metallic electrodes [67], optical microscopy of dyed tissue [73], and MEAs [4,7,68] have been used to measure the activation sequences across the surface of the heart. None of these techniques has single-cell or subcellular resolution, although such resolution, which is readily achieved with NWFETs, is crucial for better understanding cardiac function. NWFETs also can be fabricated on flexible and transparent plastic substrates [23,34,35], thus allowing conformal contact to 3D soft tissue and organs for *in-vitro* and *in-vivo* studies.

Flexible and transparent NWFETs chips that enable simultaneous optical imaging and electronic recording in configurations that are not readily accessible with traditional planar device chips were fabricated on thin polymer substrates and interfaced to beating embryonic chicken hearts [36]. A bent device chip with concave surface facing a beating heart (Fig. 8a) shows that the NWFET/heart can be readily examined with microscope. This allows for visual orientation of the device array to the heart and higher resolution imaging through the transparent substrate (Fig. 8b). Recording from the whole heart can also be realized in a convex configuration, where the heart/device interface is on the convex side of the bent chip (Fig. 8c). A representative trace recorded from the

beating heart is show in Fig. 8d [36]. The excellent SNR signal, which correlates with the spontaneous beating of the heart, shows an initial sharp peak followed by a slower phase, where these two phases can be attributed to transient ion-channel currents and mechanical motion, respectively.

These studies of acute brain slices and whole hearts demonstrate the powerful capability of NWFETs to interface with hierarchically organized tissue and organs with cellular and subcellular spatial resolution and sub-millisecond temporal resolution. Flexible NWFET chips enabled by bottom-up assembly of nanowires opens up the possibility of achieving a conformal interfaces with soft and irregularly-shaped tissues and organs, and represents substantial advantage over conventional microfabricated devices. Together these capabilities demonstrate the potential of NWFETs as tools to understand the functional connectivity and address critical biological problems in the study of neural and cardiac systems.

Intracellular electrical recording

Intracellular electrical recording, which makes a direct physical contact between probes and the interior of cells, has many advantages over extracellular recording. First, it reflects true transmembrane potential change of the cells [8,13,28,29]. Due to the capacitive nature of the cell membrane, the potential change outside the cells is normally the derivative of the cell transmembrane potential change. This makes the signal recorded by extracellular probes distinct in both amplitude and shape/time scale from the actual transmembrane potential change [6,12,51,74]. As a result, extracellular

recording reflects the time of occurrence of action potentials, but is not able to record action potentials with the details needed to explore the properties of ion channels. The opening/closing of the ion channels defines specific features/phases of an action potential recorded in intracellular (but not extracellular) measurements [1,54,75], and is fundamental to understand cellular behavior and response, for example, to drugs that interact specifically with different ion channels [2,3,76]. Second, intracellular recording can measure sub-threshold events and DC or slowly changing potentials across the cell membrane associated with synaptic interactions [8,13,28,29], which is important for neural network activity, but difficult to measure with extracellular probes. Third, intracellular recording enables precise cell-to-electrode registration. Extracellular signals often represent an average over several cells located at the vicinity of the probe. As discussed above, nanoscale extracellular probes, such as NWFETs, overcome issues of registering the position and signal to specific cell/electrode interfaces, but there is still uncertainty when a nanoscale extracellular probe is close to the boundary between cells or interfaced with subcellular structures, such as dendrites.

Conventional intracellular recording is also relatively invasive since probes must be inserted through the cell membrane. For example, commonly used glass micropipettes typically have open tip diameter of ~0.2 to 5 μm [13,75], which can be a substantial fraction of the cell size, and during recording there will be mixing of cell cytosol and exogenous filling solution (through the open tip) that cause irreversible changes to cells and make long-term measurements difficult [13,75]. Furthermore, the complexity of the glass micropipette recording makes it difficult to perform simultaneous recordings at a large number of sites. This difficulty in multiplexing also applies to sharp metal

electrodes [8,77] or carbon based microelectrodes [78,79] that have also been used as intracellular recording probes.

Our approach both to overcome the above limitations of conventional intracellular recording probes and to enable new capabilities has focused on developing novel nanoscale intracellular probes with active FET detection elements. The small sizes of these new probes, which are less than the size of viruses, allows for biomimetic approaches to be used for probe insertion, which yields non-invasive and long-term stable recording [28,29,32,33], compared with mechanical deformation of cell membranes associated with inserting much larger conventional probes [13,75]. As discussed in the section of extracellular recording, FETs can be scaled to very small ca. 10 nm scale without affecting recording capabilities [45,46], which contrasts passive metal electrodes and other potentiometric probes. However, FETs have conventionally existed in a linear geometry with S/D connections that preclude access to the inside of cells. Hence, the central issue in realizing highly scalable FET-based intracellular nanoprobes is to develop approaches where the active channel of FETs can be coupled to the inside of the cells while leaving much larger interconnects (e.g., S and D electrodes) outside the cell. We have developed two very general classes of nanoprobes based on kinked nanowire FETs [28,32] and nanotube coupled FETs [29,33] that can effectively achieve this goal and are discussed below.

Kinked nanowire FETs for intracellular recording

We have demonstrated that kinked nanowire structures in which the active FET channels is encoded at or close to the kink tip can be synthesized in a straightforward

and high-yield manner using nanocluster-catalysed growth mechanism [20]. Probes synthesized with 60° tip angle (Fig. 9a) are formed with two cis-linked 120° kinked units [28] and represent an ideal geometry for intracellular insertion, although a single 120° kink can also yield a viable probe (see below). In these nanostructures, doping modulation (upper image, Fig. 9b) was used to introduce a short channel FET topologically defined very closely to the probe tip, and heavily doped nanowire arms directly "wire-up" the FET channel as seamless nanoscale electrodes. The synthetically-defined location of the active FET channel in kinked nanowire devices was confirmed by scanning gate microscopy (SGM) measurements [20,28], where the active channel shows a large sensitivity to the gate voltage applied by the scanning tip and the heavily-doped arms are relatively insensitive. This suggested that insertion of the kink tip into a cell could readily lead to the detection of the intracellular potential variation versus time.

A complementary approach that we have implemented for making active kinked nanowire detectors involves dopant modulation during synthesis to incorporate a p-n junction near the probe tip (lower image, Fig. 9b). In this design, the active device is naturally localized at the depletion region of the p-n junction [46], where the theoretical thickness of the depletion region could be as small as 10-30 nm [80] allowing potentially very high resolution measurements. Characterization of the active region in a kinked p-n junction device by tip-modulated SGM [81] shows that the region near the kink (i.e., the position of the synthetically-defined p-n junction) exhibits a p-type gate response (Fig. 9c) [32]. The spatial resolution of the device estimated from the full width at half-maximum (FWHM) of the SGM line profiles, 210 nm, is quite good, yet lower than the theoretical limit of 10-30 nm [80], and represents an area where future improvements

could be realized.

To fabricate cellular nanoprobes using kinked nanowires, the tips must be presented in 3D from a substrate surface. Orientation of kinked nanowire probe in near vertical geometry was achieved by connecting the heavily-doped arms to free standing flexible electrodes [82] as shown in Fig. 9d [28]. The kinked nanowire geometry and extended S/D nanowire arms spatially separate the functional nanoscale FET from more bulky metal interconnects. To record the intracellular transmembrane potential change, the nanowire kink tip with active FET component must penetrate the cell membrane. To achieve penetration in a biomimetic manner we developed a new strategy based on chemical modification of the nanowires with phospholipid layers [28,29,83,84]. When phosopholipid-modified kinked nanowire probes contact a cell, the phospholipid layers could fuse with the cell membrane [85,86] and as a result, spontaneously internalize probes with a tight and high-resistance nanowire to membrane seal.

Three-dimensional phospholipid-modified kinked nanowire probes were used to record signals from spontaneously beating cardiomyocytes that were cultured on the PDMS sheets as shown schematically in Fig. 9e [28,51]. Following gentle contact between a cell and a nanowire probe, the recorded signal (Fig. 9f) exhibited several distinct features as it reached steady state [28]. First, the initial signal (~40 s) corresponded to extracellular spikes with amplitude of 3-5 mV and a submillisecond width. Second, without application of external force, the initial signal gradually disappeared with a concomitant decrease in baseline potential and occurrence of peaks with an opposite sign, similar frequency, and much larger amplitude and longer duration

of ~200 ms characteristic of the intracellular action potential of the cardiomyocytes [54,87]. The amplitude of the intracellular peaks rapidly increased during this transition period to a steady state of ~80 mV (Fig. 9g). These new steady-state intracellular action potential peaks show five characteristic phases of a cardiac intracellular potential, including (a) resting state, (b) rapid depolarization, (c) plateau, (d) rapid repolarization, and (e) hyperpolarization (Fig. 9h). In addition, a sharp transient peak (blue star, Fig. 9h) and the dip (orange star, Fig. 9h), which may be associated with the inward sodium and outward potassium currents [54], can be resolved. The evolution of signal in the recording indicates that the highly localized, point-like nanoFET near the probe tip initially records only extracellular potential, then simultaneously records both extra- and intracellular signals as the nanoFET spans the cell membrane, and finally records only intracellular signals when fully being inside the cell. The kinked nanowire probes demonstrated for the first time the FET based intracellular electrical recording, highlighted the potential of FET based intracellular tools, and provided motivation to develop other designs that exhibit unique and complementary characteristics.

Branched intracellular nanotube and active nanotube FET probes

To further reduce nanoFET intracellular probe size and make probes more scalable for high-density parallel recording, we have developed other designs using nanotube channels to bridge between the inside of cells and FET detector elements.

First, we designed a branched intracellular nanotube FET (BIT-FET, Fig. 10a) that uses a relatively conventional NWFET as the detector and an electrically-insulating nanotube that connects the FET to the cytosol or intracellular region of a cell [29]. When

there is a change in transmembrane potential V_m, such as during an action potential, the varying potential of the cytosol inside the nanotube leads to a change in FET conductance. The BIT-FET design has several unique advantages: (1) The controlled diameter nanotube to bridge to cells together with the FET based detector allows for smallest absolute probe size possible for an electrophysiology tool, and makes possible interfacing with small subcellular structure such as dendrites. (2) The external NWFET detector geometry can take advantage of the high density of those planar nanoFETs [50] to create high-density BIT-FET arrays for highly parallel recording with spatial resolution that greatly exceeds other probes [8,13].

The BIT-FET design was realized using bottom-up synthesis together with more conventional top-down processing. In short, germanium nanowire (GeNW) branches were grown on top of SiNWs, coated with a conformal, controlled-thickness SiO_2 layer [29, 88] followed by selective removal of the topmost part of the SiO_2 shell and etching of the GeNW core to yield the a hollow SiO_2 nanotube on the silicon NWFET as shown in Fig. 10b [29]. We note that the etching step used to remove the upper portion of SiO_2 results in a controlled taper at the tip due to isotropic etching of the SiO_2 shell [29], and moreover, that this taper is particularly advantageous for further decreasing probe size.

A particularly unique feature of the BIT-FET is its high bandwidth. Experimentally, pulsed water-gate measurements showed that FET conductance change followed a 0.1 ms V_{wg} pulse rise/fall without detectable delay [29], thus showing a time resolution of at least 0.1 ms. Modeling studies [29,89], which were used to estimate the bandwidth as a function of nanotube inner diameter (Fig. 10c) show that the BIT-FET

can achieve a bandwidth of ≥6 kHz, which is sufficient for recording a rapid neuronal action potential [1,13], for nanotube inner diameters as small as 3 nm [29]. The small diameters accessible with the BIT-FETs suggest that it could be minimally invasive and capable of probing the smallest cellular structures, including neuron dendrites and dendritic spines, which is difficult using conventional electrical-based techniques [5,16].

Phospholipid-modified BIT-FET probes were used to record intracellular signals from spontaneously firing embryonic chicken cardiomyocytes cells cultured on the PDMS sheets [51]. Representative data shows that approximately 45 s after gentle contact, there was a dramatic change from extracellular spikes to intracellular peaks with a concomitant baseline shift of approximately -35 mV [29, 90, 91]. Because the NWFET is p-type, the recorded intracellular conductance peaks were inverted relative to the n-type kinked nanowire probe, although the calibrated potential for these very stable peaks has the standard polarity, shape, amplitude and duration for intracellular cardiac action potential [29]. We note that the nanotubes on the BIT-FETs have very small internal volume of ~3 aL, which helps to preserve cell viability. Another unique characteristic of the BIT-FET, which distinguishes it from conventional glass micropipettes probes [13] , is that the penetration of the cell membrane and intracellular recording can be repeated on the same cell without changing position for multiple times (Fig. 10d) [29]. Indeed, we have shown that the gentle contact/intracellular recording/retraction cycle can be repeated at least five times with the same BIT-FET nanotube near the same position on a given cell without any observable change in the beating frequency and action potential features [29]. These results demonstrate unambiguously the robustness and minimal invasiveness of BIT-FET recording.

Second, we have designed a related nanotube intracellular probe in which the nanotube is a semiconductor as shown in Fig. 11a [33]. In this active silicon nanotube transistor (ANTT), insulated S and D contacts are defined on one end of the semiconducting nanotube, and the active nanotube channel is covered with insulating polymer so that only the internal part of the active channel is sensitive to solution. When the free end of the nanotube penetrates the cell membrane, the nanotube will be filled with cytosol and the ANTT probe will be sensitive to changes in the transmembrane or intracellular potential [29,33].

The ANTT probes were realized by synthesizing Ge/Si core/shell nanowires as described previously [92-94], and then etching away the Ge core with H_2O_2 [95] to leave a Si nanotube. The size of the Si nanotube probe, both the inner and outer diameter, can be tuned by changing the Ge core diameter and the Si shell thickness [33]. A representative SEM image of a 3D ANTT probe (Fig. 11b), which was fabricated in a manner similar to the kinked nanowire probe [28] described above, highlights the nanoscale dimensions and open end of the active nanotube probe. Water-gate measurements made before and after removal of the Ge nanowire core, demonstrate clearly that only the inner region of the nanotube is sensitive to potential changes. Furthermore, measurements from spontaneously firing cardiomyocytes using phospholipid-functionalized ANTT probes (Fig. 11c) showed that the probes can successfully record full-amplitude intracellular action potentials [33]. We note that the use of free-standing microscale metal electrodes to orient the ANTT probe limits its large-scale, high-density integration. This could be overcome in the future by preparing vertical nanotube FET arrays (Fig. 11d) in a manner similar to work on vertical nanowire

FETs [96,97].

Bio-mimetic, spontaneous cell membrane penetration

In all of our intracellular recording studies with the kinked nanowires [28,32], BIT-FET [29] and ANTT [33] nanoprobes, phospholipid modification was used to facilitate the cell membrane penetration and yield stable and long-term recording of full-amplitude action potentials with minimal invasiveness. The transition from extra- to intra-cellular recording, which is indicative of the probe insertion inside cells, occurs without the need to apply external forces. This behavior, which is distinct from other probes, could be attributed in part to biomimetic lipid fusion [85,86], which can occur spontaneously when the phospholipid coated nanoprobe contacts the cell membrane. The small probe sizes will be beneficial for this lipid fusion to happen. Indeed, control experiments carried out without phospholipid modification on the BIT-FETs required external forces to achieve the transition to intracellular action potential signals. Also, manipulation of a dissociated HL-1 cell [98] into contact with a kinked nanowire probe showed a clear transition to the fixed intracellular potential of the cell for phospholipid-modified probes but no internalization for unmodified probes [28].

There are several attractive consequences arising from spontaneous penetration of the phospholipid-modified nanoprobes. First, this approach typically yields full amplitude action potentials, ~75-100 mV, with our nanoprobes. The full amplitude without the need for circuitry to compensate for putative probe/membrane leakage suggests that (a) our nanoprobe is fully-internalized and (b) the nanoprobe/membrane seal is sufficiently tight to eliminate perturbing the intracellular potential (e.g., by ion leakage) [31]. Second, a

tight and stable nanoprobe/membrane seal is consistent with and explains the stable long-term intracellular recording observed in our experiments. The phospholipid modification also makes measurements less sensitive to mechanical disturbances or cell beating, and even when a phospholipid-modified nanoprobe is separated from the cell it does not result in cell death or degradation in contrast to typical case when recording with glass micropipettes [13,75]. The ability to reversibly re-insert a phospholipid-modified nanoprobe into the same (or different) cells also allows recording to be continued on scale of hours.

Third, we find that spontaneous penetration occurs in the same way for a broad range of probe orientations: for BIT-FETs, intracellular recording is achieved when nanotubes are within about 30° of the surface normal [29], and for kinked nanowire [28,32] and ANTT [33] probes angles between 40-90° can be used. This adds considerable flexibility in experimental design and robustness to the intracellular recording with our novel nanoprobes. Additional work is needed to reveal the details of the cell membrane penetration process by the phospholipid modified nanoprobes, and to elucidate the nature of the probe-membrane interface. However, the obvious advantages offered by phospholipid modification in intracellular recording with our nanoprobes validate this as a useful technique for creating robust nanoelectronics/cell interfaces.

Simultaneous, multi-site intracellular recording

A unique feature of our new nanoscale intracellular recording probes is that they enables straightforward fabrication of multiple, independent devices [99,100] for simultaneous, multi-site recording from both single cells and cell networks. One

example of the unique multiplexed recording capability of BIT-FET devices involves simultaneous recording from two nearby phospholipid-modified nanoprobes as they penetrate a single, beating cardiomyocyte (Fig. 12a) [29]. The recorded data (Fig. 12b) shows the transition to intracellular recording at different time for the two nanoprobes followed by stable full-amplitude intracellular action potentials from both devices. Multiplexed intracellular recording from a single cell was also realized with probes (Fig. 12c) in which two ANTT devices were fabricated side by side from two parallel Si nanotubes with tip-to-tip separation of ca. 7.6 μm [33]. Regular intracellular action potential peaks with 80 mV full amplitude were successfully recorded from both devices as shown in Fig. 12d [33]. In addition, we have also demonstrated the multiplexed measurements from cell networks with BIT-FET arrays [29]. Intracellular action potentials were simultaneously recorded from three devices (Fig. 12e, f) with separations sufficiently large to bridge multiple cells in a spontaneously beating monolayer of cardiomyocytes. The stable full-amplitude intracellular action potential recording from multiple nanoprobes with phospholipid modification assisted cell membrane penetration (Fig. 12f) demonstrates their flexibility and robustness compared to probe arrays requiring mechanical insertion [13,75].

Large-scale simultaneous, multi-site recording with high spatial and temporal resolution in neural and cardiac systems can contribute substantially to the fundamental understanding of network signaling and function [1,4,5,43] as well as to high-throughput drug screening [2,3]. The nanoprobes we developed and discussed in this section demonstrate an efficient way to make the high density probe arrays, and the phospholipid modification which can greatly facilitate cell membrane penetration ensures stable, long-

term recording from such nanoprobe array. We believe that the further development and application of these nanoprobes will extend substantially the scope of fundamental and applied electrophysiology studies to regimes hard to access by other methods, and contribute greatly to many areas, such as the large scale functional mapping of the brain activity with high spatio-temporal resolution, which has received intense interests recently [101].

Passive metal electrode based intracellular probes

In addition to our active FET based intracellular probes, several groups have been exploring on-chip metal electrodes for intracellular action potential recording [102-106]. First, Spira and coworkers [102-104] have fabricated arrays of micrometer-sized protruding gold-spine microelectrodes which were functionalized with a peptide containing multiple Arg-Gly-Asp (RGD) repeats. This peptide, named engulfment-promoting peptide (EPP9), facilitates the engulfment of the gold spine electrodes by the membrane of the cultured neurons thus forming a high resistance seal. Recording from the engulfed gold-spine electrodes following glass micropipette stimulation of nearby or the same cells yielded subthreshold synaptic and action potential signals from individual neurons. From a representative measurement, the amplitude of the 'raw' action potentials recorded by different spine electrodes was 0.1–25 mV, which is smaller than the value simultaneously recorded with a glass micropipette [103]. Differences in the signal amplitude from different electrodes could arise from variations of the electrode impedance and/or the electrode/cell membrane coupling [103], and the difficulty of controlling these factors could make quantitative interpretation of multi-site recording

difficult.

Two subsequent studies that have extended these ideas to smaller dimension electrodes [105,106] have utilized similar device designs consisting either of an array of Pt [105] or Si [106] vertical nanowires with diameter of ~150 nm, lengths of 1.5 and 3 μm for each electrode. In the case of the PtNWs array, HL-1 cells were cultured on the electrodes. Recording from spontaneously beating HL-1 cells initially yielded small ~100–200 μV extracellular spikes, but following voltage pulse (2.5 V; 200 μs) the signal transitions to one similar to an intracellular action potential albeit with a reduced amplitude of ~11.8 mV [105]. The authors suggest that the voltage pulse induces nanometer-sized pores [107-110] thereby providing access to the intracellular potential. In the case of the SiNWs array, where the nanowires tips were capped with a sputter-deposited metal to make the passive recording electrode, HEK293 and rat cortical neurons were cultured on the electrodes [106]. Measurements suggested that some nanowires electrodes spontaneously penetrated HEK293 cell membranes during culture although for others, a large voltage pulse (~±3 V; duration, 100 ms) was needed to yield intracellular signals [106]. Voltage pulses from the SiNWs array electrode can also be used to evoke action potentials in the rat cortical neurons. However, signals recorded with the SiNWs array electrode were smaller in amplitude than that simultaneously recorded with the glass patch pipette [106].

The above works represent a substantial advance in on-chip metal electrodes for recording intracellular-like action potentials. The use of metal based electrode can also deliver stimulatory pulses in addition to potential change recording

[103,106], which was not demonstrated for the FET based nanoprobes. However, the high impedance at the metal electrode/electrolyte interface limits the ultimate size of these probes. For example, it will be hard for the micrometer-scale gold spine electrode to record from small subcellular features such as dendrite, and although each nanowire in the nanowires array has 100-200 nm diameters, reliable recording typically requires multiple nanowires per electrode. During the recording, all the nanowires on the electrode are needed to be inside the cell (any nanowire remaining outside the cell will lead to a leakage). This leaves a typical projected area on the micrometer scale for these electrodes [105,106]. Moreover, as reported by these works [103,106], high electrode impedance and/or other factors can lead to a distortion of signal shapes and attenuation of signal amplitude, which might limit analysis of data recorded simultaneously from multiple sites. The use of direct engulfment during culture to assist getting intracellular or 'in-cell' recording is helpful in getting high-resistance sealing and preserving cell viability. But the electroporation induced access to cell interior is transient and can only last several minutes [105,106], and multiple use of electroporation or current injection is damaging to cell viability [106]. Overall, these factors represent challenges that must be overcome in the development of such passive nanoelectrode approaches. In future, new device design which can be used for both stimulation and recording with true nanoscale precision and resolution will be important for comprehensive study of neuronal circuits, and in this regard, we suggest that 'impedance-free' FET detection with stimulatory capabilities will be a promising direction for the future.

Three-dimensional nanoelectronics/tissue hybrids

One unique feature of the bottom-up paradigm emphasized in this review is the capability to design and realize nanodevices and networks not possible by conventional methods [23]. In this section, we will discuss our work of developing macroporous, flexible and free-standing nanoelectronic scaffolds (nanoES), the application of the nanoES as biocompatible extracellular scaffolds for 3D culture of neurons, cardiomyocytes and smooth muscle cells, and the recording of electrical activity, pH sensing and drug responses monitoring within these electronically-innervated tissue constructs [39].

Implementing electrical sensors in 3D and the capabilities for monitoring cells throughout the 3D micro-environment of tissues is critical for understanding cellular activity and physicochemical change relevant to living organisms [111-113]. Most of current work directed towards coupling electronics with tissue has focused on coupling to the surface of natural tissues/organs or artificial tissue constructs, including recently reported studies using flexible and/or stretchable electronics that conform to tissue surfaces [36,40,41]. Previous works have been limited in terms of merging electronics with tissues throughout 3D space with minimal tissue disruption, because the 2D support structures and the electronic sensors are generally on much larger scale than the extracellular matrix (ECM) and cells. Seamlessly merging electronics throughout tissues has been recently realized with our introduction of the nanoES concept as outlined in Fig. 13 [39] , which addresses key constraints: (1) The electronic structures must be macroporous, not planar, to enable 3D interpenetration with biomaterials and cells; (2) the electronic network should have nanometer to micrometer scale features with comparable size to biomaterial scaffolds; and (3) the electronic network must have 3D

interconnectivity and mechanical properties similar to biomaterials. As shown schematically in Fig. 13 [39], after depositing kinked or straight nanowires on surface, individual NWFET devices were lithographically patterned into a network (steps A and B, Fig. 13), and then released from the underlying substrate to yield free-standing nanoES. The 3D nanoES network have nanometer to micrometer features and high (>99%) porosity, and are also highly flexible and biocompatible. The resulting nanoES, which can be combined with traditional macroporous ECMs to form a hybrid scaffold (step B, Fig. 13) or used alone, is then seeded with cells and cultured (step C, Fig. 13) to yield 3D nanoelectronic–tissue hybrids.

We have made two kinds of nanoES and used them for the creation of innervated tissues with neurons, cardiomyocytes and smooth muscle cells. First, a reticular nanoES [39], was designed with bimetallic metal interconnects such that upon relief from the substrate it self-organizes into a 3D electrically interconnected scaffold with kinked nanowire sensors [39]. Reconstructed 3D confocal fluorescence images of a typical reticular scaffold (Fig. 14a) shows clearly the 3D interconnected structure. SEM images (Fig. 14b) further demonstrate that the size of the passivated metallic interconnects and polymeric structural ribbons are all ≤ 1 μm in width, and thus comparable with synthetic and natural ECMs [111].

We cultured embryonic rat hippocampal neurons in this type of reticular nanoES following merging with a conventional scaffold, Matrigel [39]. Reconstructed 3D confocal micrographs from a two-week culture (Fig. 14 c, d), show clearly neurons with a high density of spatially interconnected neurites that penetrate seamlessly the reticular

nanoES (Fig. 14c), sometimes passing through the ring structures supporting individual NWFETs (Fig. 14d). Standard LIVE/DEAD cell assay [114] further demonstrated that the viability of hippocampal neurons cultured in the reticular nanoES/Matrigel versus the control Matrigel over 21 days was the same within experimental error. This shows that on the 2-3 week timescale, the nanoES component of the scaffolds has little effect on the cell viability. Furthermore, the original NWFET device characteristics were retained after the scaffold hybridization and following cell culture. The capability of the nanoES for long-term culture and monitoring enables a number of in vitro studies, including drug screening assays with these synthetic neural tissues.

The second basic class of nanoES we developed is termed the mesh nanoES. In mesh nanoES, we define a regular NWFET devices array with structural backbone and use unstrained metal interconnects such that upon relief from the substrate, a flexible, free-standing macroporous nanodevice sheet is formed. Three dimensional scaffolds were then realized in a straightforward manner by directed manipulation, such as folding and loosely stacking adjacent mesh layers, rolling the sheets, or by shaping it with other biomaterials [39]. The porosity of the mesh nanoES is comparable to that of a honeycomb-like synthetic ECM engineered for cardiac tissue culture [115], thus making it an ideal scaffold for innervating synthetic cardiac tissue.

Significantly, 3D cardiac tissue was achieved from a hybrid mesh nanoES/PLGA (poly(lactic-co-glycolic acid) scaffolds following seeding and culture of cardiomyocytes [39]. Confocal fluorescence microscopy of a typical cardiac 3D culture (Fig. 14e) revealed a high density of cardiomyocytes in close contact with the nanoES components.

Striations characteristic of cardiac tissue [115,116] can be observed from epifluorescence micrographs of cardiac cells on the surface of the nanoES cardiac patch (Fig. 14f). Similar to the 3D nanoES/neural tissue, cytotoxicity tests showed minimal difference in cell viability for culture in the hybrid mesh nanoES/Matrigel/PLGA and Matrigel/PLGA [39].

Electrical recording from NWFET devices within nanoES/cardiac tissue hybrid (Figs. 14g, h) demonstrate the sensory capabilities of the nanoES. For example, recording from a NWFET ~200 μm below the construct surface gave regularly spaced spikes with a frequency of ~1 Hz, a calibrated potential change of ~2-3 mV, a SNR ≥3 and a ~2 ms width. The peak amplitude, shape and width are consistent with extracellular recordings from cardiomyocytes. Following dosage of the construct with noradrenaline (also known as norepinephrine), which is a drug that stimulates cardiac contraction [54], the recorded signal showed a twofold increase in frequency. We note that SiNW FETs at different position in the cardiac patch show response to the noradrenaline application at different time scale. This provides us a way to study the drug effect from 3D tissue models, and thus demonstrates its potential as a platform for *in vitro* pharmacological studies, which is expected to provide a more robust link to *in vivo* disease treatment than that can be achieved from 2D cell cultures [111,117,118]. In addition, multiplexed sensing from a coherently beating nanoES/cardiac construct (Fig. 14h) demonstrated submillisecond temporal resolution from four NWFETs with separations up to 6.8 mm within the 3D innervated tissue sample [39].

One additional example demonstrating the power of our new paradigm centers on the development of innervated vascular constructs (Fig. 15a) with embedded nanoelectronic sensory capabilities [39]. Human aortic smooth muscle cells (HASMCs) were cultured on 2D mesh nanoES, and then the hybrid nanoES/HASMC sheets (Fig 15b) were rolled into multi-layer 3D tubular structures as shown in Fig 15c [39]. This process is analogous to that used for tissue-engineered autologous blood vessels [119,120] except for the key addition of the nanoES, which provides real-time sensory capability in 3D. The smooth muscle tissue was ~200 μm thick with elongated cells and collagenous nanofibres, and embedded nanoES, as revealed from analyses of haemotoxylin–Eosin- and Masson-trichrome-stained sections (Fig. 15d). Notably, 3D pH sensing measurements in which constant pH solution was flowed through the inside (lumen) region of the vascular construct and extravascular solution pH was varied stepwise (Fig. 15e) showed several key features. First, the NWFETs in the outermost layer showed stepwise conductance decreases with a sensitivity of ~32mV per pH unit. Second, only minor baseline fluctuations were observed for the NWFETs in the innermost layer (closest to lumen). This result demonstrated the potential ability of the embedded NWFETs to detect inflammation, ischemia, tumor micro-environments or other forms of metabolic acidosis [121,122] in the implanted devices, which is important to many aspects of biomedical research and healthcare.

The work with nanoES represents a new paradigm and direction for interfacing nanoelectronics with biological systems in 3D, where the coupling extends from the surface to inside the biological samples, and is distinct from either engineered

tissue [111,123] or flexible electronics [37,40,41]. Although the implantation of these nanoES-embedded synthetic tissues for *in vivo* studies will require substantial work, the sensing capabilities throughout the 3D micro-environment of the tissue constructs provides exciting possibility for studying the pharmacological response of cells within synthetic tissues, and for localized and real-time monitoring of cellular activities and physicochemical change in 3D.

Conclusions and outlook

This review has summarized recent progress in interfacing nanoelectronics with biological systems at different levels, from nanoscopic recording probes for cultured cells, tissue slices and whole organs, to 3D nanoelectronics-tissue hybrids. Pictorially, these advances and opportunities are summarized in Fig. 16. The newly developed extra- and intra-cellular recording probes and related technique enable minimally-invasive, long-term, high spatio-temporal resolution measurements of action potentials in neural and cardiac systems. The 3D implementation of functional electronic devices in artificial tissue or tissue constructs further allows for localized, real-time monitoring of cellular electrical activity and physicochemical change from the inside of the tissue. All of these results represent great advances in nanoelectronics-biology interfacing, and will serve as the foundation for new fundamental studies and novel directions in biomedical research and applications.

One promising application of the 2D and 3D nanoscopic probes for action potential recording discussed in this review is for large scale mapping of neural activity. Functional mapping of brain activity has received intense interests recently [101].

To explore the brain function it will be important to create high-density nanoprobes, which by virtue of their small sizes, allow for minimally-invasive and high spatial resolution measurement in both 2D and more importantly 3D space. Although the nanoprobes reviewed here have not been prepared yet on a massive scale, the multiplexed measurements discussed in this article already demonstrate the substantial capabilities of them and the potential for integrating on a larger scale. Moreover, the new 3D recording capability demonstrated with the macroporous free-standing 3D nanoprobes is expected to open up a new vista for large scale, deep tissue or brain activity recording which is difficult with other methods [39-41]. Further development of high throughput fabrication schemes for these 2D and 3D nanoprobes will be needed for this direction. Expanding our nanoprobe concepts by including additional types of functional devices, such as nanoscale light-emitting diodes and stimulators, as well as integrating wireless interfaces will further increase their power and capabilities for mapping brain activity.

More generally, the integrating of multiple functions, including (i) electrical and photo stimulating devices, (ii) detectors for chemical and biochemical species such as small molecules and proteins, (iii) strain sensors for mechanical stress and other physical properties of the biological sample, and (iv) drug releasing devices that provide feedback to the physicochemical change of the synthetic tissue, promise to have a profound impact on biophysical and electrophysiological research [111]. Electrical stimulating provides temporally precise control of neuronal activity [1,31]. Current stimulating technique involves the use of large size glass micropipette [1] or sharp metal electrodes [8,77], which lack the spatial precision needed and are invasive to the biological systems. This calls for nanoscale stimulating devices and the integration of them with the FET based

nanoscale recording probes. Incorporation of photonic materials for efficient light-addressable interfaces with photoactive cells [124,125] is another aspect to further extend the scope of nanoelectronics-biology coupling. Proper tissue function and regeneration rely on robust spatial and temporal control of biophysical and biochemical micro-environmental cues [126-128]. Integrating not only sensors for these cues, but also the feedback loops, such as the drug releasing devices which responds to these cues, is important to maintain fine control at the cellular and tissue level over the synthetic tissue growth and function [128].

The development of such multi-functional nanodevices and interfacing them with different biological systems will advance fundamental biophysical research and open up new biomedical applications. Neuronal dendrites provide the vast majority of the surface area in most neurons and receive the majority of neuron's synaptic input [66]. However, their small diameters have made direct electrical measurements difficult. Recently, some key advances have been made using intracellular sharp microelectrode recordings [129-131], but this approach is very difficult and also does not permit simultaneous, multi-site recording. The small size of our novel nanoscale probes, together with the capability for high-density, large-scale integration of multiple probes, makes them appealing and well suited for studies in this key area. We believe that developing our novel nanoscale probes as high-density multiplexed recording platforms will enable measurements from these subcellular neuronal axons and dendrites which will greatly advance the study of synaptic plasticity and information flow in neural networks.

Biomaterials embedded with functional devices, with both detection and regulating capabilities, could provide new and exciting possibilities for stem cell studies [128]. Stem cells are considered the most versatile and promising cell source for the regeneration of aged, injured and diseased tissues [132]. Different biomaterials are being used to build model systems to mimic the features of stem cell microenvironments in order to study the roles of biochemical and physical signaling [128]. Our seamless embedding of functional devices using the nanoES could enable detection of the critical biochemical information of niche components, and also biophysical properties such as matrix mechanical properties. The incorporation of delivery devices could allow the identity, concentration and patterns of molecules, which are of biological relevance to stem cell regulation, to be defined. All of these will be important to understand extrinsic regulators of stem cell fate and ultimately, help to achieve control over stem cell differentiation or propagation.

Finally, nanodevices that form intimate extra- or intra-cellular connections with excitable cells and tissue are expected to advance substantially functional prosthetics used to address medical conditions such as spinal cord injuries [133] and blindness [134]. Less invasive interaction between nanoscale devices and biological systems, including the advances such as the nanoES, should allow us to overcome issues that exist with conventional devices, such as delamination of the metallic electrode surface and inflammation and astrocyte accumulation in the surrounding tissue [135-139]. By utilizing the nanoscale functional elements in implantable devices or nanoES/tissue hybrids, it could be possible to create, for example, a retinal prosthesis where the stimulating resolution, pixel number and cross-coupling to other neurons are greatly

improved. One can envision nanoES-based implantable tissues that are hard wired to provide closed-loop systems that sense and respond, enable telemetric monitoring of physiological processes, and/or provide connections to the host nervous system. Truly exciting opportunities for the future!

Acknowledgements

This work was supported by NIH Director's Pioneer Award (5DP1OD003900), McKnight Foundation Technological Innovations in Neurosciences Award, National Security Science and Engineering Faculty Fellow (NSSEFF) award (N00244-09-1-0078), and"National Thousand Talents Plan " award from China.

References

[1] B. Hille, Ion Channels of Excitable Membranes, third ed., Sinauer Associates Inc., Sunderland, 2001.
[2] J. Dunlop, M. Bowlby, R. Peri, D. Vasilyev, R. Arias, Nature Rev. Drug Discov. 7, 358-368 (2008).
[3] T. Meyer, K. H. Boven, E. Gunther, M. Fejtl, Drug Safety, 27 (2004) 763-772.
[4] S. Dhein, F. W. Mohr, M. Delmar, Practical Methods in Cardiovascular Research, Springer-Verlag, Berlin, 2005, pp. 215-453.
[5] J. T. Davie, M. H. P. Kole, J. J. Letzkus, E. A. Rancz, N. Spruston, G. J. Stuart, et al., Nat. Protoc. 1 (2006) 1235-1247.
[6] J. Erickson, A. Tooker, Y.-C. Tai, J. Pine, J. Neurosci. Method. 175 (2008) 1-16.
[7] M. Reppel, F. Pillekamp, Z. J. Lu, M. Halbach, K. Brockmeier, B.K. Fleischmann, et al., J. Electrocardiol. 37 (2004) 104-109.
[8] R. D. Purves, Microelectrode Methods for Intracellular Recording and Ionophoresis, Academic Press Inc., Burlington, 1981.
[9] Yeung, S. Ingebrandt, M. Krause, A. Offenhausser, W. Knoll, J. Pharmacol. Toxicol. Methods. 45 (2001) 207-214.

[10] A. Cohen, J. Shappir, S. Yitzchiak, M. E. Spira, Biosens. Bioelectron. 22 (2006) 656-663.
[11] A. Cohen, J. Shappir, S. Yitzchaik, and M. E. Spira, Biosens. Bioelectron. 23 (2008) 811-819.
[12] M. Voelker, P. Fromherz, Small 1 (2005) 206-210.
[13] A. Molleman, Patch Clamping: An Introductory Guide to Patch Clamp Electrophysiology, Wiley, 2003.
[14] O. J. Prohaska, F. Olcaytug, P. Pfundner, H. Dragaun, IEEE Trans.Biomed. Eng. BME-33 (1986) 223-229.
[15] D. J. Banks,W. Balachandran, P. R. Richards, D. Ewins, Physiol. Meas. 23 (2002) 437-448.
[16] M. Scanziani, M. Hausser, Nature 461 (2009) 930-939.
[17] J. T. Hu, T. W. Odom, C. M. Lieber, Acc.Chem. Res. 32 (1999) 435-445.
[18] W. Lu, C. M. Lieber, J. Phys. D.: Appl. Phys., 39 (2006) R387-R406.
[19] C. M. Lieber, Z. L.Wang, MRS Bull., 32 (2007) 99-104.
[20] B. Tian, P. Xie, T.J. Kempa, D.C. Bell, C.M. Lieber, Nature Nanotech. 4 (2009) 824-829.
[21] X. Jiang, B. Tian, J. Xiang, F. Qian, G. Zheng, H. Wang, et al., Proc. Natl. Acad. Sci. USA 108 (2011) 12212-12216.
[22] C. Thelander, P. Agarwal, S. Brogersma, J. Eymery, L. F. Feiner, A. Forchel, et al., Mater. Today, 9 (2006) 28-35.
[23] W. Lu, C. M. Lieber, Nature Mater. 6 (2007) 841-850.
[24] Y. Cui, Q. Wei, H. Park, C. M. Lieber, Science, 293 (2001) 1289-1292.
[25] G. Zheng, F. Patolsky, Y. Cui, W. U. Wang, C. M. Lieber, Nature Biotechnol., 23 (2005) 1294-1301.
[26] B. P. Timko, T. Cohen-Karni, Q. Qing, B. Tian C.M. Lieber, IEEE Trans. Nanotechnol. 9 (2010) 269-280.
[27] F. Patolsky, B. P. Timko, G. Yu, Y. Fang, A. B. Greytak, G. Zheng, et al., Science 313 (2006), 1100-1104.
[28] B. Tian, T. Cohen-Karni, Q. Qing, X. Duan, P. Xie, C.M. Lieber, Science 329 (2010) 831-834.
[29] X. Duan, R. Gao, P. Xie, T. Cohen-Karni, Q. Qing, H.S. Choe, et al., Nature Nanotech. 7 (2012), 174-179.
[30] J. F. Eschermann, R. Stockmann, M. Hueske, X. T. Vu, S. Ingebrandt, A. Offenhäusser Appl. Phys. Lett., 95 (2009) 083703-1-083703-3.
[31] W. L. C. Rutten, Annu. Rev. Biomed. Engl. 4 (2002), 407-452.
[32] Z. Jiang, Q. Qing, P. Xie, R. Gao, C.M. Lieber, Nano Lett. 12 (2012) 1711-1716.
[33] R. Gao, S. Strehle, B. Tian, T. Cohen-Karni, P. Xie, X. Duan, et al., Nano Lett. 12 (2012) 3329-3333.

[34] A. Javey, S. Nam, R. S. Friedman, H. Yan, C. M. Lieber, Nano. Lett., 7 (2007) 773-777.
[35] M. C. McAlpine, R. S. Friedman, S. Jin, K. Lin, W. Wang, C. M. Lieber, Nano Lett., 3 (2003) 1531-1535.
[36] B. P. Timko, T. Cohen-Karni, G. Yu, Q. Qing, B. Tian, C. M. Lieber, Nano. Lett., 9 (2009) 914-918.
[37] T. Cohen-Karni, Q. Qing, Q. Li, Y. Fang, C.M. Lieber, Nano Lett. 10 (2010), 1098-1102.
[38] C. Bai, M. Liu, Nano Today, 7 (2012) 258-281.
[39] B. Tian, J. Liu, T. Dvir, L. Jin, J.H. Tsui, Q. Qing, et al., Nature Mater. 11 (2012) 986-994.
[40] J. Viventi, D.-H. Kim, L. Vigeland, E. S. Frechette, J. A. Blanco, Y.-S. Kim, et al. Nat. Neurosci. 14 (2011), 1599-1605.
[41] D.-H. Kim, N. Lu, R. Ma, Y.-S. Kim, R.-H. Kim, S. Wang, et al. Science 333 (2011), 838-843.
[42] D. A. Wagenaar, J. Pine, S. M. Potter, BMC Neurosci. 7 (2006): 11.
[43] U. Egert, D. Heck, A. Aertsen, Exp. Brain Res. 142 (2002) 268-274.
[44] Y. Zhang, I. J. Kim, J. R. Sanes, M. Meister, Proc. Natl. Acad. Sci. USA. 109 (2012) E2391-8.
[45] F. Patolsky, G. Zheng, C. M. Lieber, Anal. Chem. 78 (2006) 4260-4269.
[46] S. M. Sze, K. K. Ng, Physics of Semiconductor Devices, 3rd ed. Wiley Interscience, 2006.
[47] L. G. Nowak, J. Bullier, Exp. Brain Res., 118 (1998) 477-488.
[48] M. H. P. Kole, S. U. Ilschner, B. M. Kampa, S. R. Williams, P. C. Ruben, G. J. Stuart, Nat. Neurosci., 11 (2008) 178-186.
[49] M. H. P. Kole, G. J. Stuart, Nat. Neurosci. 11 (2008) 1253-1255.
[50] H. Yan, H.S. Choe, S.W. Nam, Y. Hu, S. Das, J.F. Klemic, et al., Nature 470 (2011) 240-244.
[51] T. Cohen-Karni, B.P. Timko, L.E. Weiss, C.M. Lieber, Proc. Natl. Acad. Sci. USA 106 (2009) 7309-7313.
[52] S. Ingebrandt, C.-K. Yeung, M. Krause, A. Offenhausser, Biosens. Bioelectron. 16 (2001) 565-570.
[53] A. G. Kleber, Y. Rudy, Physiol. Rev., 84 (2003) 431-488.
[54] D. P. Zipes, J. Jalife, Cardiac Electrophysiology: From Cell to Bedside, fifth ed., Saunders, Philadelphia, 2009.
[55] A. K. Geim, Science, 324 (2009) 1530-1534.
[56] A. K. Geim, K. S. Novoselov, Nature Mater. 6 (2007) 183-191.
[57] Y. Hu, J. Xiang, G. Liang, H. Yan, C. M. Lieber, Nano Lett. 8 (2008) 925-930.
[58] C. Yang, Z. Zhong, C.M. Lieber, Science 310 (2005) 1304-1307.

[59] T. Cohen-Karni, D. Casanova, J. Cahoon, Q. Qing, D. Bell, C.M. Lieber, Nano Lett. 12 (2012) 2639-2644.
[60] S. Kodambaka, J. Tersoff, M. C. Reuter, F. M. Ross, Science 316 (2007) 729-732.
[61] C. Y. Wen, M. C. Reuter, J. Bruley, J. Tersoff, S. Kodambaka, E. A. Stach, et al., Science 326 (2009) 1247-1250.
[62] V. Schmidt, J. V. Wittemann, U. Gösele, Chem. Rev. 110 (2010) 361-388.
[63] C. W. Yang, Z. Zhong, C. M. Lieber, Science 310 (2005) 1304-1307.
[64] T. E. Clark, P. Nimmatoori, K.-K. Lwe, L. Pan, J. M. Redwing, E. C. Dickey, Nano Lett. 8 (2008) 1246-1252.
[65] V. G. Fast, A. G. Kleber, Circ. Res. 75 (1994) 591-595.
[66] G. M. Shepherd, The Synaptic Organization of the Brain fifth Ed. Oxford Univ Press, Inc., New York, 2004, Ch. 1, 5, 10, 11.
[67] B. Taccardi, B. B. Punske, E. Macchi, R. S. LacLeod, P. R. Ershler, Am. J. Physiol.: Heart Circ. Physiol. 294 (2008) H1753.
[68] Z.-L. Lu, A. Pereveraev, H.-L. Liu, M.Weiergr¨aber, M. Henry, A. Krieger, et al., Cell. Physiol. Biochem., 14 (2004) 11-22.
[69] Q. Qing, S.K. Pal, B. Tian, X. Duan, B.P. Timko, T. Cohen-Karni, et al., Proc. Natl. Acad. Sci. USA 107 (2010) 1882-1887.
[70] C. Wirth, H. R. Lüscher , J Neurophysiol. 91 (2004) 1635-1647.
[71] U. Frey, U. Egert, F. Heer, S. Hafizovic, A. Hierlemann Biosens Bioelectron, 24 (2009) 2191-2198.
[72] C. Stangl, P. Fromherz, Eur J Neurosci. 27 (2008) 958-964.
[73] I. R. Efimov, V. P. Nikolski, G. Salama, Circ. Res. 94 (2004) 21-33.
[74] J. Pine, J. Neurosci. Methods 2 (1980) 19-31.
[75] B. Sakmann, E. Neher, Single-Channel Recording, 2nd ed. Springer, 2009.
[76] W. Zheng, R. H. Spencer, L. Kiss, Assay Drug Dev. Technol. 2 (2004) 543–552.
[77] D. H. Hubel, Science 125 (1957) 549-550.
[78] M. G. Schrlau, N. J. Dun, H. H. Bau, ACS Nano 3 (2009) 563-568.
[79] E. D. De Asis, J. Leung, S. Wood, C. V. Nguyen, Appl. Phys. Lett. 95 (2009) 153701.
[80] L. Weber, E. Gmelin, Appl. Phys. A 53 (1991) 136-140.
[81] N. R. Wilson, D. H. Cobden, Nano Lett. 8 (2008) 2161-2165.
[82] T. G. Leong, C. L. Randall, B. R. Benson, N. Bassik, G. M. Stern, D. H. Gracias, Proc. Natl. Acad. Sci. U.S.A. 106 (2009) 703-708.
[83] N. Misra, J. A. Martinez, S.-C. Huang, Y. Wang, P. Stroeve, C. P. Grigoropoulos, et al., Proc. Natl. Acad. Sci. U.S.A. 106 (2009) 13780-13784.
[84] C. A. Keller, K. Glasmästar, V. P. Zhdanov, B. Kasemo, Phys. Rev. Lett. 84 (2000) 5443-5446.

[85] B. D. Almquist, N. A. Melosh, Proc. Natl. Acad. Sci. U.S.A. 107 (2010) 5815-5820.
[86] L. V. Chernomordik, M. M. Kozlov, Nature Struct. Mol. Biol. 15 (2008) 675-683.
[87] D. M. Bers, Nature 415 (2002) 198-205.
[88] D., Hausmann, J. Becker, S. Wang, R. G. Gordon, Science 298 (2002) 402-406.
[89] M. N. O. Sadiku, Elements of Electromagnetics third ed., Oxford Univ. Press, 2000.
[90] R. P. Buck, E. S. Grabbe, Anal. Chem. 58 (1986) 1938-1941.
[91] I. Tasaki, I. Singer, Ann. NY Acad. Sci. 148 (1968) 36-53.
[92] B. Tian, X. Zheng, T.J. Kempa, Y. Fang, N. Yu, G. Yu, et al., Nature 449 (2007) 885-890.
[93] B. Tian, T. J. Kempa, C. M. Lieber, Chem. Soc. Rev., 38 (2009) 16-24.
[94] T.J. Kempa, J.F. Cahoon, S.-K. Kim, R.W. Day, D.C. Bell, H.-G. Park et al., Proc. Natl. Acad. Sci. USA 109 (2012) 1409-1412.
[95] M. Ben-Ishai, F. Patolsky, J. Am. Chem. Soc. 131 (2009) 3679-3689.
[96] J. Goldberger, A. I. Hochbaum, R. Fan, P. Yang, Nano Lett. 6 (2006) 973-977.
[97] T. Bryllert, L. Wemersson, L. E. Froberg, L. Samuelson, IEEE Electron Device Lett. 27 (2006) 323-325.
[98] W. C. Claycomb, N. A. Lanson, Jr., B. S. Stallworth, D. B. Egeland, J. B. Delcarpio, A. Bahinski et al., Proc. Natl. Acad. Sci. U.S.A. 95 (1998) 2979.
[99] D. Whang, S. Jin, Y. Wu, C. M. Lieber, Nano Lett. 3 (2003) 1255-1259.
[100] A. Javey, S. Nam, R.S. Friedman, H. Yan, C.M. Lieber, Nano Lett. 7 (2007) 773-777.
[101] C. Koch, R. C. Reid, Nature 483 (2012) 397-398.
[102] A. Hai, A. Dormann, J. Shappir, S. Yitzchaik, C. Bartic, G. Borghs, et al., J. R. Soc. Interface 6 (2009) 1153-1165.
[103] A. Hai, J. Shappir, M. E. Spira, Nature Methods 7 (2010) 200-202.
[104] A. Hai, J. Shappir, M. E. Spira, J. Neurophysiol. 104 (2010) 559-568.
[105] C. Xie, Z. Lin, L. Hanson, Y. Cui, B. Cui, Nature Nanotech. 7 (2012), 185-190.
[106] J. T. Robinson, M. Jorgolli, A. K. Shalek, M-H. Yoon, R. S. Gertner, H. Park, Nature Nanotech. 7 (2012) 180-184.
[107] N. Akaike, N. Harata, Jpn. J. Physiol. 44 (1994) 433-473.
[108] U. Zimmermann, G. Pilwat, F. Riemann, Biophys. J. 14 (1974) 881-899.
[109] E. Neumann, M. Schaeferridder, Y. Wang, P. H. Hofschneider, EMBO J. 1 (1982) 841-845.
[110] D. C. Chang, T. S. Reese, Biophys. J. 58 (1990) 1-12.

[111] T. Dvir, B. P. Timko, D. S. Kohane, R. Langer, Nature Nanotech. 6 (2011) 13-22.
[112] J. Viventi, D.-H. Kim, J. D. Moss, Y.-S. Kim, J. A. Blanco, N. Annetta, et al., Sci. Transl. Med. 2 (2000) 24ra22.
[113] M. A. L. Nicolelis, (ed.) Methods for Neural Ensemble Recordings, second ed. CRC Press, 2008.
[114] T. Xu, P. Molnar, G. Cassie, M. Das, T. Boland, J. J. Hickman. Biomaterials 30 (2009) 4377-438.
[115] G. C. Jr Engelmayr, M. Cheng, C. J. Bettinger, J. T. Borenstein, R. Langer, L. E. Freed, Nature Mater. 7 (2008) 1003-1010.
[116] Y. Sapir, O. Kryukov, S. Cohen, Biomaterials 32 (2011) 1838-1847.
[117] T. P. Kraehenbuehl, R. Langer, L. Ferreira, Nature Methods 8 (2011) 731-736.
[118] D. W. Hutmacher, Nature Mater. 9 (2010) 90-93.
[119] N. L'Heureux, S. Pâquet, R. Labbé, L. Germain, F. A. Auger, FASEB J. 12 (1998) 47-56.
[120] N. L'Heureux, N. Dusserre, G. Konig, B. Victor, P. Keire, T. N. Wight, et al., Nature Med. 12 (2006) 361-365.
[121] D. Neri, C. T. Supuran, Nature Rev. Drug Discov. 10 (2011) 767-777.
[122] J. A. Kraut, N. E. Madias, Nature Rev. Nephrol. 6 (2010) 274-285.
[123] T. Dvir, B. P. Timko, M. D. Brigham, S. R. Naik, S. S. Karajanagi, O. Levy, et al., Nature Nanotech. 6 (2011) 720-725.
[124] T. C. Pappas, W. M. S. Wickramanyake, E. Jan, M. Motamedi, M. Brodwick, N. A. Kotov, Nano. Lett., 7 (2007) 513-519.
[125] J. Liu, C. Xie, X. Dai, L. Jin, W. Zhou, C. M. Lieber, Proc. Natl. Acad. Sci. USA 110 (2013), 6694-6699.
[126] D. E. Discher, D. J. Mooney, P. W. Zandstra, Science 324 (2009) 1673-1677.
[127] F. Guilak, D. M. Cohen, B. T. Estes, J. M. Gimble, W. Liedtke, C. S. Chen, Cell Stem Cell 5 (2009) 17-26.
[128] M. P. Lutolf, P. M. Gilbert, H. M. Blau, Nature 462 (2009) 433-441.
[129] R. Llinas, C. Nicholson, J. Neurophysiol. 34 (1971) 532-551.
[130] R.K. Wong, D.A. Prince, A.I. Basbaum, Proc. Natl. Acad. Sci. USA 76 (1979) 986-990.
[131] R. Llinas, M. Sugimori, J. Physiol. 305 (1980) 197-213.
[132] H. M. Blau, A. Sacco, P. M. Gilbert, in Encyclopedia of Stem Cell Research (eds Svendsen, C. & Ebert, A.), Sage Publications, Inc., 2008.
[133] S. F. Gizler, Neurotherapeutics 5 (2008) 147-162.
[134] A. Caspi, J. D. Dorn, K. H. McClure, M. S. Humayun, R. J. Greenberg, M. J. McMahon, Arch. Opthalmol. 27 (2009) 398-401.

[135] Z. Yu, O. Graudejus, C. Tsay, S.P. Lacour, S. Wagner, B. Morrison III, J.Neurotrauma 26 (2009) 1135-1145.
[136] S. F. Cogan, A. A. Guezelian,W. F. Agenw, T. G. H. Yuen, D. B. Mc-Greery, J. Neurosci. Methods, 137 (2004) 141-150.
[137] J. D.Yeager, D. J. Phillips, D. M. Rector, D. F. Bahr, J. Neurosci. Methods 173 (2008) 279-285.
[138] D. H. Szarowski, M. D. Andersen, S. Retterer, A. J. Spence, M. Isaacson, H. G. Craighead, et al., Brain Res. 983 (2003) 23-25.
[139] R. Biran, D. C. Martin, P. A. Tresco, Exp. Neurol. 195 (2005) 115-126.

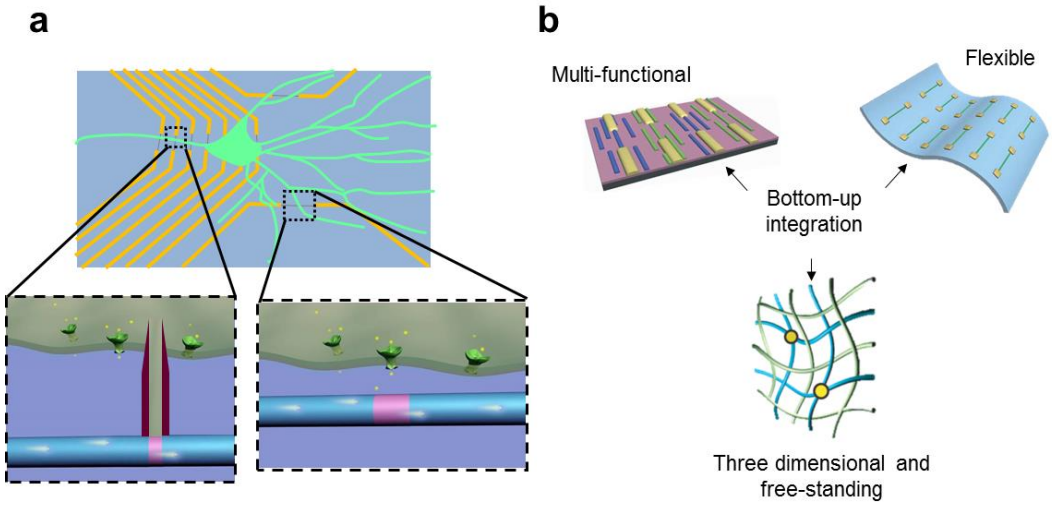

Figure 1 Schematic illustration of the advantages for using SiNW based devices to interface with biological systems. (a) SiNW based devices are used for intra- and extracellular action potential recording. The small size of the functional element increases the spatial precision and resolution, also enables subcellular interfacing; (b) The bottom-up pathway used for making the nanoscale electronic devices allows us to realize multi-function on a single chip, make flexible electronics, also three-dimensional and free-standing devices to interface from inside the tissue.

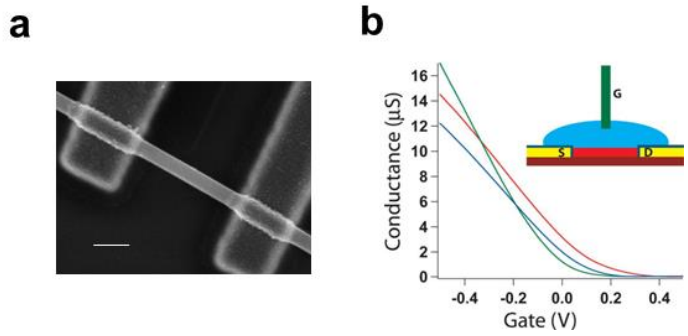

Figure 2 SiNW based FET biosensors. (a) Scanning electron microscope image of a SiNW FET. Scale bar is 100 nm; (b) Conductance versus water-gate voltage trace for three representative SiNW FET devices. Inset: Scheme representing experimental setup, (red) nanowire, (yellow/navy) passivated contact electrodes, (blue) electrolyte solution, (green) Ag/AgCl reference/gate electrode.

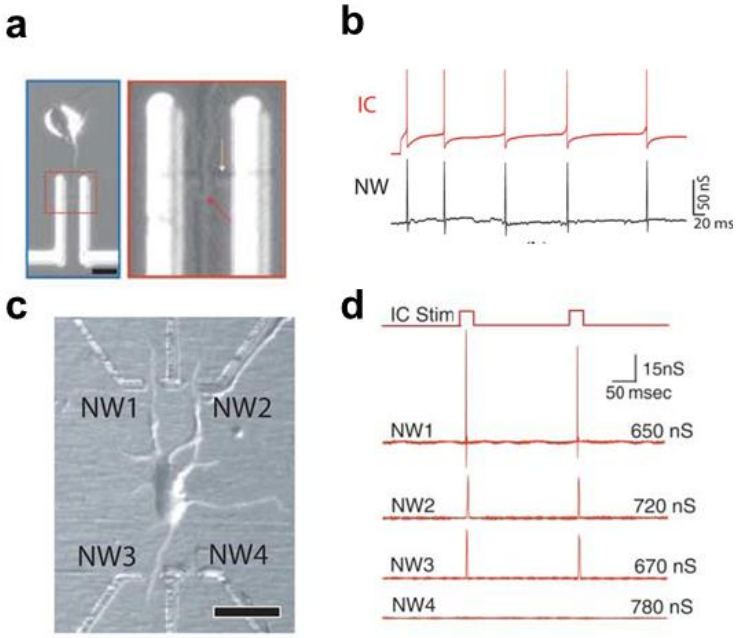

Figure 3 Extracellular action potential recording from cultured neurons. (a) Left: optical image of a cortical neuron aligned across a SiNW FET; scale bar is 10 µm. Right: High-resolution image of the region where axon (red arrow) crosses a SiNW (yellow arrow). (b) Red trace: intracellular potential of an cortex neuron (after 6 days in culture) recorded by glass micropipette during stimulation; Black trace: time-correlated signal

from axon measured using a p-type SiNW FET; (c) Optical image of a cortical neuron interfaced to three of the four functional NWFETs in an array; scale bar is 20 µm; (d) Trace of intracellular current stimulation and resulting electrical responses from the four SiNW FETs in *c*. Reprinted with permission from Ref. [27]. Copyright 2006 American Association for the Advancement of Science.

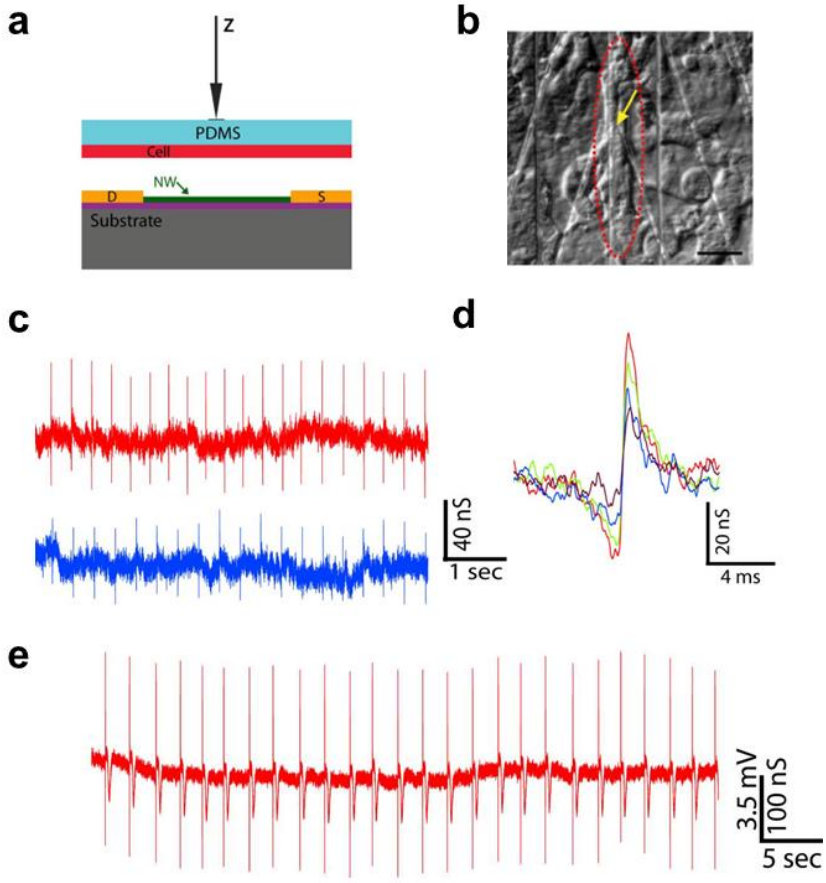

Figure 4 Building interface between SiNW FETs and spontaneously firing cardiomyocytes. (a) Schematic illustration of manipulating the PDMS/cell substrate to make the interface with an NWFET device. (b) Distinct patch of beating cells (red dashed oval) over a SiNW device (yellow arrow). scale bar is 20 µm; (c) Two representative traces recorded with same SiNW FET from a spontaneously firing cardiomyocyte with different PDMS/cell displacement value; (d) High resolution comparison of single peaks recorded with increasing displacement values (from purple to red); (e) Data recorded in distinct experiment at displacement value close to cell failure. Reprinted with permission from Ref. [51]. Copyright 2009 National Academy of Sciences.

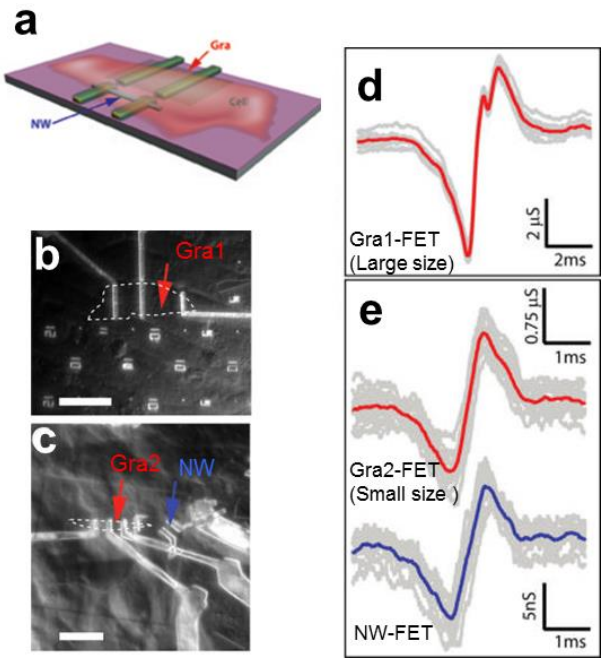

Figure 5 Extracellular action potential recording from nanoFETs with different projection area. (a) Schematic illustrating the chip design incorporating graphene and SiNW FET devices; (b) Optical microscope image of PDMS/cells interfaced with large flake graphene FET. Graphene flake outline is marked by white dashed line; measured device is marked by red arrow. Scale bar is 30 μm; (c) Optical microscope image of PDMS/cells interfaced with smaller flake graphene FET and SiNW FET. Graphene flake outline is marked by white dashed line, measured graphene device is marked by red arrow, and measured SiNW device is marked by blue arrow. Scale bar is 13.6 μm; (d) Recorded averaged peak (red) and raw data (gray traces) for the Gra1-FET and cell in *b*; (e) Thirteen raw signal peaks (gray traces) from the Gra2-FET (upper data) and SiNW FET (lower data) devices marked by red and blue arrows, respectively in *c*. The average of the peaks was plotted in red and blue, respectively. Reprinted with permission from Ref. [37]. Copyright 2010 American Chemical Society.

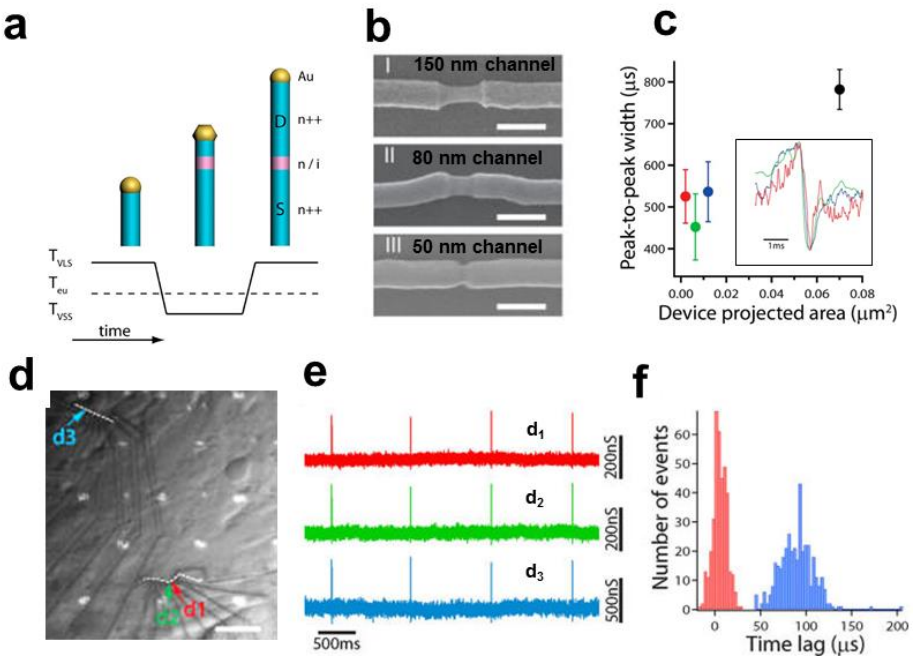

Figure 6 Extracellular action potential recording with short channel NWFETs. (a) Illustration of Au-nanocluster-catalyzed nanowire growth with well-controlled axial dopant profile introduced during VSS growth; (b) Short-channel $n^{++}/i/n^{++}$ SiNWs with channel lengths of 150 nm, 80 nm, and 50 nm respectively. Scale bars are 150 nm. The Au-nanoclusters were ~80 nm in diameter, and nanowires were selectively etched to reveal the active channel; (c) Summary of the peak-to-peak widths for the 150, 80, and 50 nm channel length devices. In addition, a previously published 2.3 µm channel length SiNW device (black) is shown for comparison [37]. Inset, an example of single peaks from each of the short-channel devices; (d) Optical image of cardiomyocytes interfaced with three 130 nm channel length devices (labeled d1, d2, and d3). White dashed lines illustrate the nanowire position. Scale bar is 15 µm; (e) Representative recorded signals from the three devices in *d*; (f) Histogram of the time lag between devices d1 and d2 (red; separation distance 1.9 µm) and between devices d1 and d3 (blue; separation distance 73 µm). Reprinted with permission from Ref. [59]. Copyright 2012 American Chemical Society.

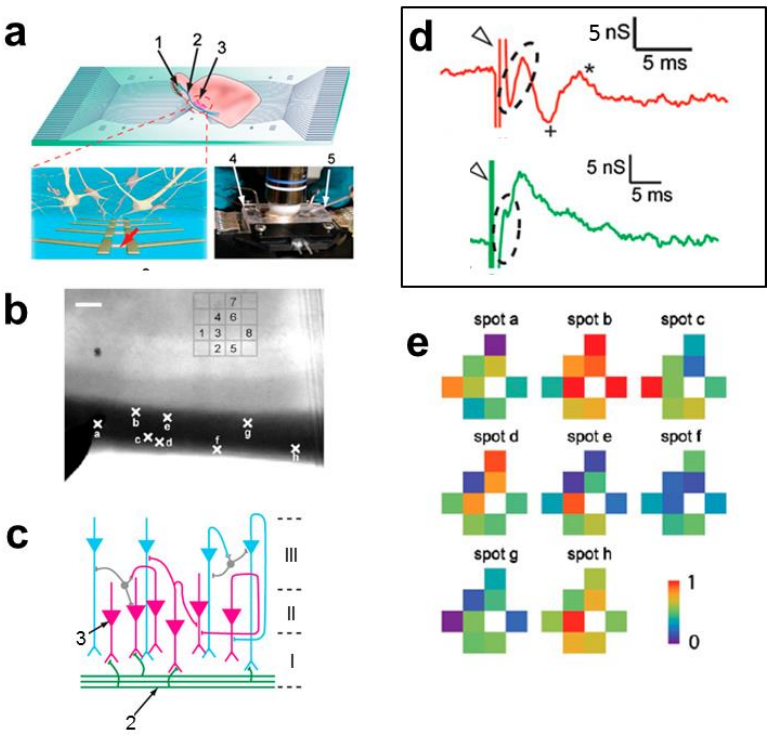

Figure 7 Extracellular field and action potential recording from brain slices with NWFETs. (a) Measurement schematics. Top: overview of a NWFET array interfacing with slice oriented with pyramidal cell layer over the devices. Bottom Left: zoom-in of device region illustrating interconnected neurons and NWFETs. Bottom Right: photograph of the assembled sample chamber. 1, 2, and 3 indicate the mitral cells in the olfactory bulb, the lateral olfactory tract, and the pyramidal cells, respectively. 4 and 5 mark the stimulation electrode and the patch clamp pipette, respectively; (b) Optical image of an acute slice over a 4 × 4 NWFET array. Crosses along the LOT fiber region of the slice mark the stimulation spots a-h. Scale bar is 100 µm; (c) Laminar organization and input circuitry of the piriform cortex (Layer I–III); (d) a zoom-in signal recorded from two SiNW FET devices. The Open Triangle and Dashed Oval mark the stimulation and presynaptic features, resp. The Plus and Asterisk mark the postsynaptic features; (e) Maps of the relative signal intensity or activity for devices 1–8. Reprinted with permission from Ref. [69]. Copyright 2010 National Academy of Sciences.

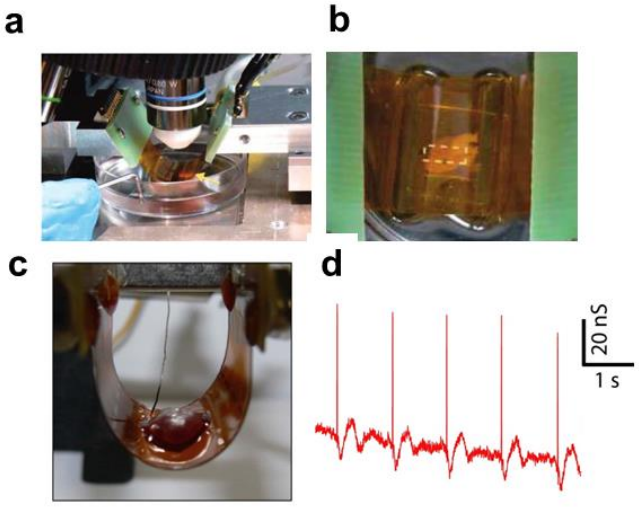

Figure 8 Action potential recording from whole hearts with NWFETs fabricated on flexible plastic substrate. (a) Photograph of a flexible SiNW FETs chip interfaced with a chicken heart in concave configuration. Yellow arrow marks the location of the heart; (b) Top-down photograph of same system, which enables overall registration between heart and lithographically defined markers on the substrate; (c) Photograph of a flexible SiNW FETs chip interfaced with a chicken heart in convex configuration; (d) A representative recorded conductance data from a SiNW FET interfacing with chicken heart in bent configuration. Reprinted with permission from Ref. [36]. Copyright 2009 American Chemical Society.

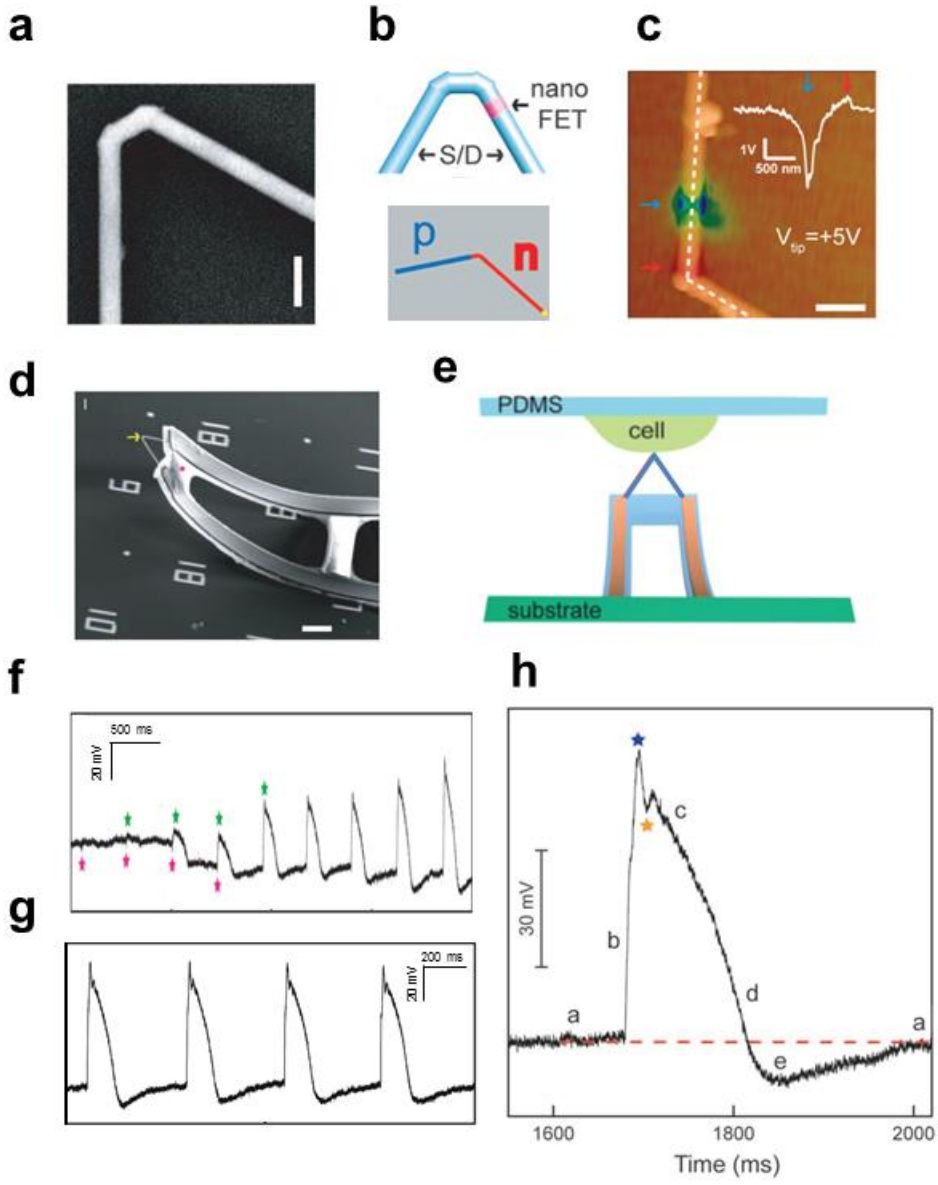

Figure 9 Intracellular action potential recording with kinked nanowire FET devices. (a) SEM image of a doubly kinked nanowire with a cis configuration. scale bar: 200 nm; (b) Top: schematic of kinked nanowire probe with encoded active region (pink) by dopant level modulation. The blue regions designate the source/drain (S/D). Low: schematic of kinked nanowire probe with p-n junction; (c) Superposition of tmSGM images on AFM topographic images of a representative kinked p–n nanowire device under V_{tip} of +5 V. Scale bar is 0.5 µm. The blue/red arrows indicate the p-type and n-type depletion/ accumulation regions (left panel), respectively. Inset: line profile of the tmSGM signal along the white dashed lines; (d) A 3D, free-standing kinked nanowire FET probe bent up by stress release of the metal interconnects. The yellow arrow and pink star mark the

nanoscale FET and SU-8, respectively. Scale bars, 5 µm; (e) Schematic of intracellular recording from spontaneously beating embryonic chicken cardiomyocytes cultured on PDMS substrate using kinked nanowire nanoprobes; (f) Transition from extracellular to intracellular recordings during cellular entrance recorded by a kinked nanowire FET probe from beating cardiomyocytes. Green and pink stars denote the peak positions of intracellular and extracellular signal components, respectively; (g) Steady-state intracellular recording; (h) Zoom-in signals of an intracellular action potential peak. Blue and orange stars designate features that are possibly associated with inward sodium and outward potassium currents, respectively. The letters 'a' to 'e' denote five characteristic phases of a cardiac intracellular potential, as defined in text. The red-dashed line is the baseline corresponding to intracellular resting state. Reprinted with permission from Ref. [28][32]. Copyright 2010 American Association for the Advancement of Science, 2012 American Chemical Society.

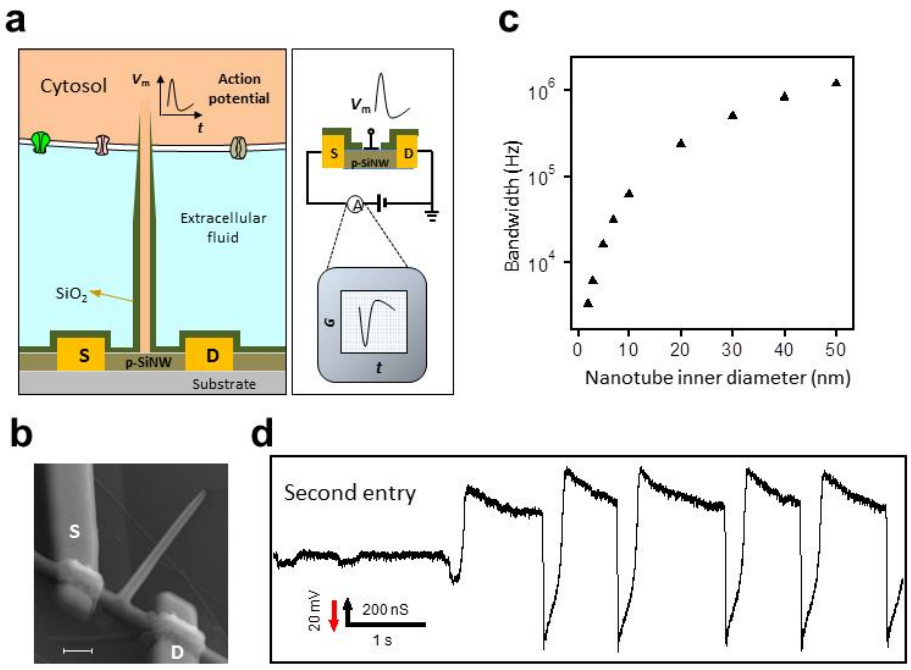

Figure 10 Intracellular action potential recording with the BIT-FET. (a) Schematics illustrating the working principle of intracellular electrical recording with the BIT-FET; (b) SEM image of a BIT-FET device. Scale bar is 200 nm; (c) Calculated bandwidth of the BIT-FET device versus the inner diameter of the nanotube (ALD SiO2 thickness was the same

as the nanotube inner diameter, and the nanotube length was fixed at 1.5 μm); (d) A representative trace corresponding to the second entry of the nanotube from a BIT-FET around the same position on the cardiomyocyte cell. Reprinted with permission from Ref. [29]. Copyright 2012 Nature Publishing Group.

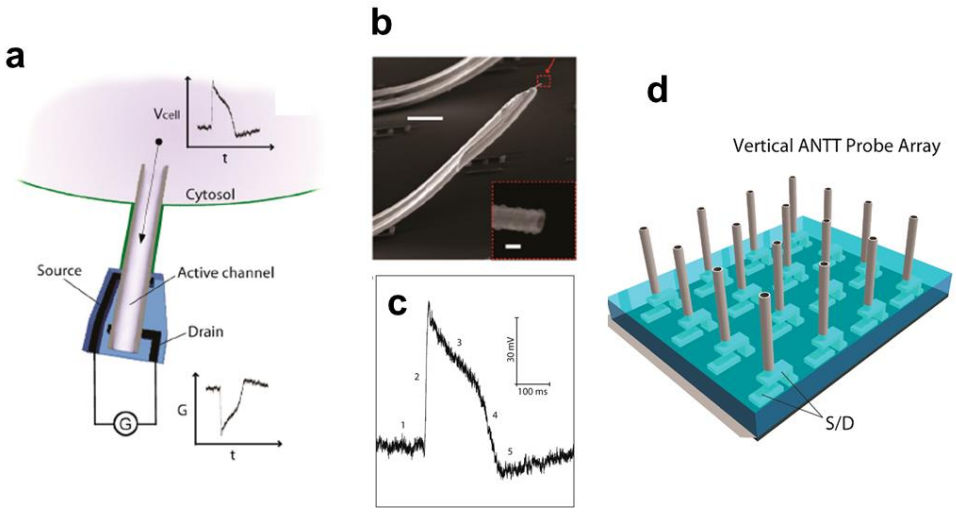

Figure 11 Intracellular action potential recording with the ANTT. (a) Schematic illustration the working principle of intracellular electrical recording with the ANTT; (b) SEM image of an ANTT probe. Scale bar, 10 μm. Inset, zoom of the probe tip from the dashed red box. Scale bar, 100 nm; (c) A representative intracellular action potential peak recorded with an ANTT. The five characteristic phases of the action potential peak are denoted by 1−5; (d) Schematic of chip-based vertical ANTT probe arrays fabricated from epitaxial Ge/Si nanowires for enhanced integration. Reprinted with permission from Ref. [33]. Copyright 2012 American Chemical Society.

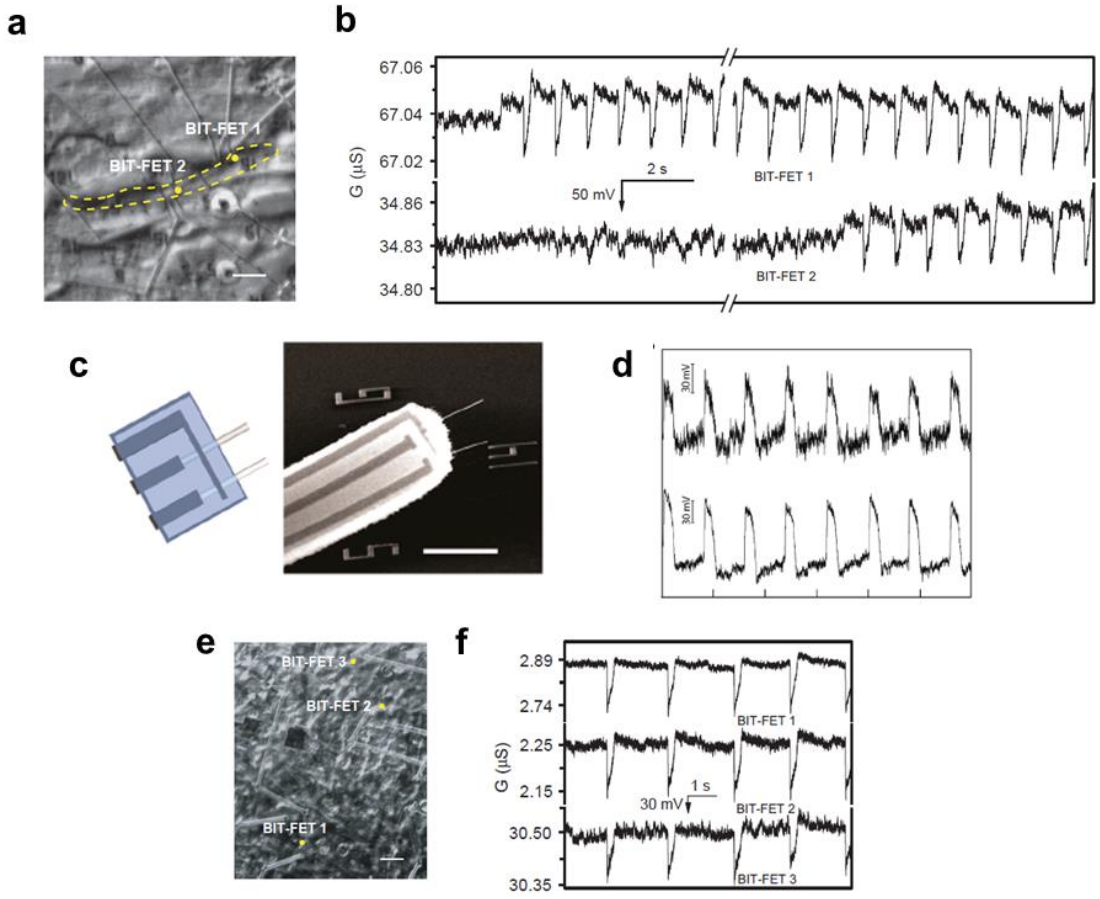

Figure 12 Multiplexed intracellular action potential recording. (a) Optical image of two BIT-FET devices (positions marked with dots) coupled to a single cardiomyocyte cell, with the cell boundary marked by the yellow dashed line. Scale bar is 10 µm; (b) Simultaneously recorded traces from the two devices in a, corresponding to the transition from extracellular to intracellular recording; (c) Design and SEM image of a probe with two independent ANTT devices sharing a common source contact. Horizontal

scale bar, 5 µm; (d) Intracellular recording from a single cardiomyocyte using a probe with two independent ANTT devices. The interval between tick marks corresponds to 1 s; (e) Optical image of three BIT-FET devices coupled to a beating cardiomyocyte cell network. Scale bar is 30 µm; (f) Representative traces recorded simultaneously from the devices shown in e. Reprinted with permission from Ref. [29][33]. Copyright 2012 Nature Publishing Group, 2012 American Chemical Society.

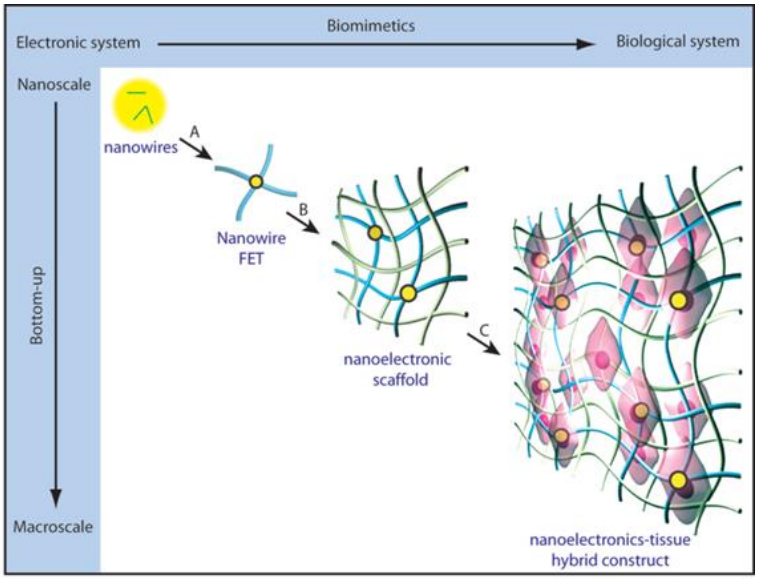

Figure 13 Merging nanoelectronics with artificial tissues seamlessly for three-dimensional electrical interfacing. Reprinted with permission from Ref. [39]. Copyright 2012 Nature Publishing Group.

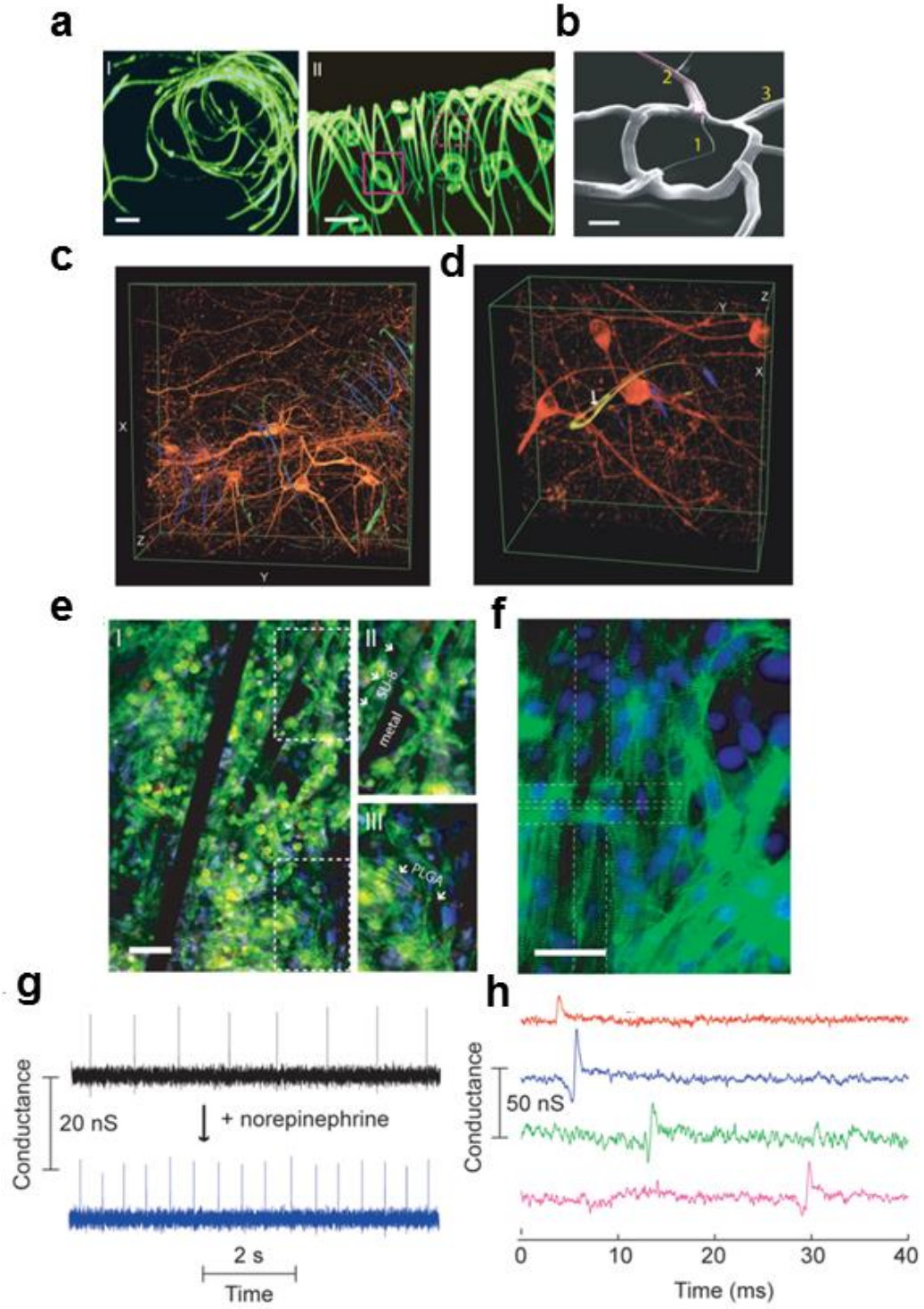

Figure 14 Nanowire nanoES, 3D nanoelectronics/tissue hybrids, and 3D action potential recording. (a) 3D reconstructed confocal fluorescence micrographs of reticular nanoES

viewed along the y (I) and x (II) axes. Solid and dashed open magenta squares indicate two nanowire FET devices located on different planes along the x axis. The overall size of the structure, x–y–z=300–400–200 μm. Scale bars, 20 μm; (b) SEM image of a single kinked nanowire FET within a reticular scaffold, showing (1) the kinked nanowire, (2) metallic interconnects (dashed magenta lines) and (3) the SU-8 backbone. Scale bar, 2 μm; (c, d) 3D reconstructed confocal images of rat hippocampal neurons after a two-week culture on reticular nanoES/Matrigel. The white arrow highlights a neurite passing through a ring-like structure supporting a nanowire FET. Dimensions in c, x: 317 μm; y: 317 μm; z: 100 μm; in d, x: 127 μm; y: 127 μm; z: 68 μm; (e) Confocal fluorescence micrographs of a synthetic cardiac patch. (II and III), Zoomed-in view of the upper and lower dashed regions in I, Scale bar, 40 μm; (f) Epifluorescence micrograph of the surface of the cardiac patch. Green: α-actin; blue: cell nuclei. The dashed lines outline the position of the S/D electrodes. Scale bar, 40 μm; (g) Conductance versus time traces recorded from a single NW FET before (black) and after (blue) applying noradrenaline; (h) Multiplexed electrical recording of extracellular field potentials from four nanowire FETs at different depth in a mesh nanoES/cardiac hybrid. Data are conductance versus time traces of a single spike recorded at each nanowire FET. Reprinted with permission from Ref. [39]. Copyright 2012 Nature Publishing Group.

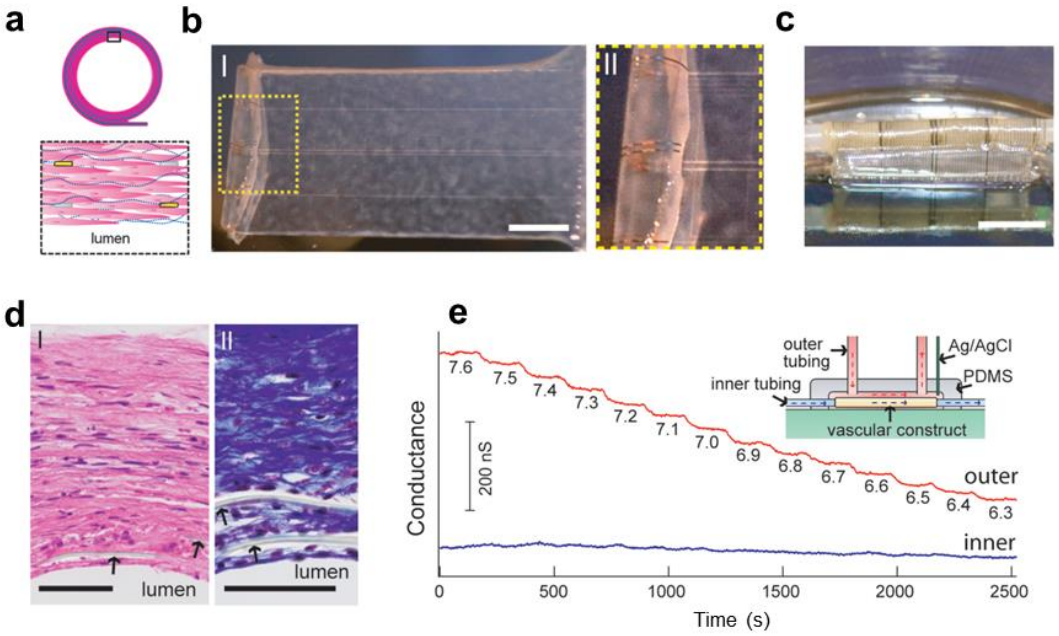

Figure 15 Synthetic vascular construct enabled 3D sensing. (a) Schematic of the smooth muscle nanoES. The upper panels are the side view, and the lower one is a zoom-in view. Grey: mesh nanoES; blue fibers: collagenous matrix secreted by HASMCs; yellow dots: nanowire FETs; pink: HASMCs; (b) (I) Photograph of a single HASMC sheet cultured with sodium L-ascorbate on a nanoES. (II) Zoomed-in view of the dashed area in I. Scale bar, 5 mm; (c) Photograph of the vascular construct after rolling into a tube and maturation in a culture chamber for three weeks. Scale bar, 5 mm; (d) Haematoxylin–Eosin- (I) and Masson-Trichrome- (II; collagen is blue) stained sections (~6 µm thick) cut perpendicular to the tube axis; lumen regions are labelled. The arrows mark the positions of SU-8 ribbons of the nanoES. Scale bars, 50 µm; (e) Changes in conductance over time for two nanowire FET devices located in the outermost (red) and innermost (blue) layers. The inset shows a schematic of the experimental set-up. Outer tubing delivered bathing solutions with varying pH (red dashed lines and arrows); inner tubing delivered solutions with fixed pH (blue dashed lines and arrows). Reprinted with permission from Ref. [39]. Copyright 2012 Nature Publishing Group.

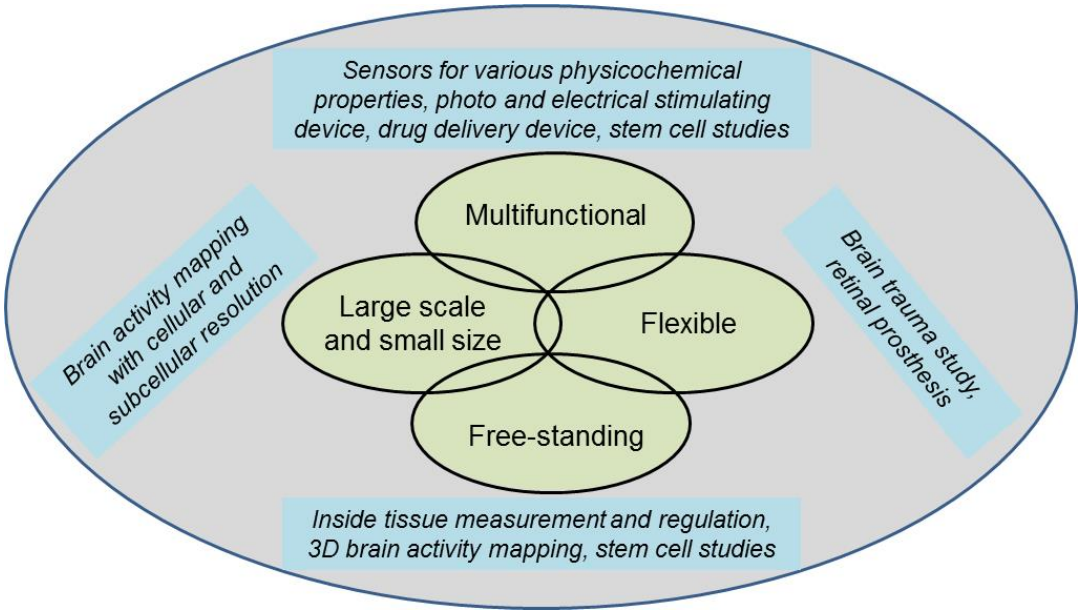

Figure 16 Overview of nanoelectronics-biology interfacing enabled new fundamental studies and novel directions in biomedical research and applications. These new studies benefit from different features of the nanoelectronics.